Received: 21 August 2020 | Revised: 13 March 2021 | Accepted: 24 March 2021

IET Smart Grid

DOI: 10.1049/stg2.12041

The Institution of Engineering and Technology WILEY

ORIGINAL RESEARCH PAPER

Key performance-cost tradeoffs in smart electric vehicle charging with distributed generation

John W. Heron[1] | Hongjian Sun[1,2] | Omid Alizadeh-Mousavi[3] | Andrew Crossland[2]

[1]Department of Engineering, Durham University, Durham, UK

[2]Durham Energy Institute, Durham University, Durham, UK

[3]DEPsys SA, Puidoux, Switzerland

Correspondence

John W. Heron and Hongjian Sun, Department of Engineering, Durham University, Stockton Road, Durham, England, DH1 3LE, United Kingdom.
Email: john.w.heron@durham.ac.uk and hongjian.sun@durham.ac.uk

Funding information

European Commission Horizon 2020, Grant/Award Number: 734325; Engineering and Physical Sciences Research Council, Grant/Award Number: EP/P005950/1; Engineering and Physical Sciences Research Council United Kingdom

Abstract

Growing penetration of Electric Vehicles (EV) and Distributed Generation (DG) is driving sharper peaks in demand and supply, which, if poorly managed, manifest as over- or undervoltage and disrupt grid service quality. Smart charging schemes reschedule EV charging load according to factors such as grid stability, price signals, etc. It remains unclear how to do this while meeting the diverging needs and expectations of multiple concerned participants. This paper proposes two smart charging schemes for secondary voltage control in the distribution network and analyses performance-cost tradeoffs relating to key players in the Smart Grid. To support these schemes, a distributed communications architecture is designed that jointly minimises traffic burden, computation load and investment in Information and Communications Technology (ICT) hardware. Scheme I (Smart Curtailment), curtails load and DG for peak shaving. Scheme II (Smart Correction) optimises cost-efficiency for subscribing users by maximising power transfer during off-peak hours or when renewable energy is high. Performance of both schemes is consolidated statistically under almost 6 months of practical input profiles. Dramatic improvements in EV & DG capacity are demonstrated and key performance-cost tradeoffs relating to Voltage Control, Peak Shaving, User Inconvenience, CO_2 Emissions and ICT Deployment Cost are identified.

1 | INTRODUCTION

The United Kingdom (UK) government plans for all cars sold to be purely electric by 2030 [1]. Owning an Electric Vehicle (EV) will cause a significant increase in household energy consumption. Typical UK households consume roughly 5–20 kWh/day [2], while a typical EV battery capacity ranges 20–100 kWh [3–6]. Further, synchronised driving patterns are plausible, for example numerous EVs require immediately charging upon returning home from work. All this points to sharper peaks in consumer power demand. Predicted effects of random uncoordinated charging in the power network range from significant to disastrous [7–9].

Meanwhile, increased environmental awareness has motivated a surge in renewable Distributed Generation (DG), fed directly into the distribution network alongside consumers. In 2019, the share of renewable generation in annual electricity supply reached a record high of 37% in the UK [10]. By 2050, the National Grid expects that 42% of all generation will be connected at the distribution level [11, 12]. Unlike traditional electric power sourced from municipal power plants, renewable energy is highly dependent on weather conditions and is non-synchronised with consumer demand. Changes in weather can lead to sudden peaks or troughs in power conditions for which the distribution network is not necessarily designed [13–15].

If poorly managed, sharp peaks in supply and demand manifest as over- or under-voltage conditions that can trigger passive protection elements, mandatory load shedding and blackouts. They can also lead to grid congestion, increased line losses, overloading of transformers, feeders and protection equipment as well as high harmonic distortion that is invisible to the network operator. For this reason, limits are placed on DG, typically 15%–20% of peak load [16].

Smart charging techniques seek to mitigate localised imbalances by exploiting the discretionary power requirement of EVs: it does not matter exactly when charging takes place, so long as it is charged when the consumer requires. Thus it is

possible, within certain timing constraints, to adjust net demand according to grid stability requirements.

There has been some work in this field. In [17], a smart charging approach using the assigned phase of loads is presented to achieve superior loss minimisation performance. In [8], an EV charging scheme with distributed wind power cost-efficiently meets consumer charging requirements based on real-time pricing. Peak shaving under EV load curves incorporating distributed solar power is analysed in [18]. A fuzzy logic based EV charging strategy in [19] keeps minimum bus voltage within operating limits. A fast-converging distributed demand-response method is proposed in [20] to minimise peak demand. In [21], two independent compensation mechanisms for LV feeder voltage control with EVs and solar DG are compared. An algorithm based on charging time zone priorities in [7] improves the voltage profile, where 63% EV penetration could be tolerated with no peak load increase. A bi-directional EV and DG control concept is presented in [22] for grid support services. The impact of various EV charging strategies on distribution grids with wind generation is studied in [9], and excellent reviews on infrastructural challenges of smart charging are presented [23, 24].

The literature exposes three critical areas for research. First, smart charging can be sought from two optimisation objectives:

(A) For peak shaving in the network [7, 17–20]. Power equipment, which is sized according to the peak load, can then be minimally supplemented to accommodate the rising demand. Equipment can be operated closer to its limits and power efficiency more effectively optimised, reducing technical losses and operating costs.
(B) To maximise power transfer when it is cheap, that is during non-peak times or when renewable generation is high [8, 22].

However, these two objectives **A** and **B** can be misaligned [9]. High renewable generation can lead to cheap electricity during peak loading hours. In this case, when smart charging demand reacts to the cheaper energy prices it can lead to a very high peak load in the network. In this case, the operator desires peak shaving, while consumers/generators desire peak charging. This paper explicitly answers this dichotomy.

Second, it remains unclear how to guarantee satisfaction for the multiple concerned power network participants. In [20], EV owners input a deadline before which a certain amount of charge must be stored in their EV batteries. In [7], users select a priority band within which their vehicle will charge. Practically, smart charging is possible via user subscription, where EV owners are compensated for potential charging delay with cheaper energy prices. User inconvenience must be correctly matched with compensation to maintain high subscription numbers. Further, costs relating to infrastructure investment and scheme implementation must be balanced against overall benefits. DG curtailment reduces return on investment in renewable generation, disincentivising its instalment. Smart Grid services stand to uproot the conventional economic structure of power distribution. This paper explicitly models key performance-cost tradeoffs relating to diverse expectations of all concerned participants.

Third, practical Information and Communications Technology (ICT) constraints inherent in the operation of any Smart Grid system are routinely overlooked in smart charging research. Perfect knowledge of grid status, energy prices, driving patterns and loading is generally assumed everywhere in the network, and that any actuating device can act with zero latency. Where delay is mentioned, for example [25, 26], it refers to convergence time and/or control action period of the optimisation scheme, not that of sensor hardware, bandwidth and traffic constraints due to practical ICT investment budgets. Cost of data collection is a key constraint. This paper designs an underpinning control and communications architecture such that traffic burden, computation at the central controller and investment in ICT hardware are all jointly minimised.

The contributions of this paper are as follows:

- Two smart charging schemes are designed relevant to divergent design objectives of operator and consumer/generator. Both achieve secondary voltage control in the distribution network and simultaneous increase in EV & DG capacity. Scheme I for peak shaving. Scheme II to maximise cost-efficiency for consumers and DG investors.
- A multi-tier hierarchical distributed control architecture is designed to support these schemes. This alleviates computation load on the central controller as well as traffic load on the ICT system, and is compatible with existing open smart charging and demand-response communications standards such as Open Charge Point Protocol (OCPP) and Open Automated Demand Response (OpenADR). Therefore the schemes are scalable and adaptable to a wide variety of network sizes and asset arrangements, and are readily applicable to the industrial environment.
- Practical operational latency constraints are analysed and modelled, and multiple latency-mitigation strategies are identified for each smart charging scheme.
- Performance of both schemes is consolidated statistically for 172 days of 1s wind power input. Key performance-cost tradeoffs are identified relating to Voltage Control, Peak Shaving, User Inconvenience, CO_2 Emissions and Cost of ICT Deployment.

The rest of this paper is laid out as follows. Section 2 describes the testbed system model, outlining key inputs and the underpinning communications architecture. Scheme I is described in Section 3 along with critical operation elements under ideal and practical latency. Scheme II is described in Section 4. In Section 5, four control variables are identified that determine voltage control performance under practical latency, and a case study for each is provided. Key performance-cost tradeoffs are evaluated statistically from simulation in Section 6, before Section 7 concludes the topic.

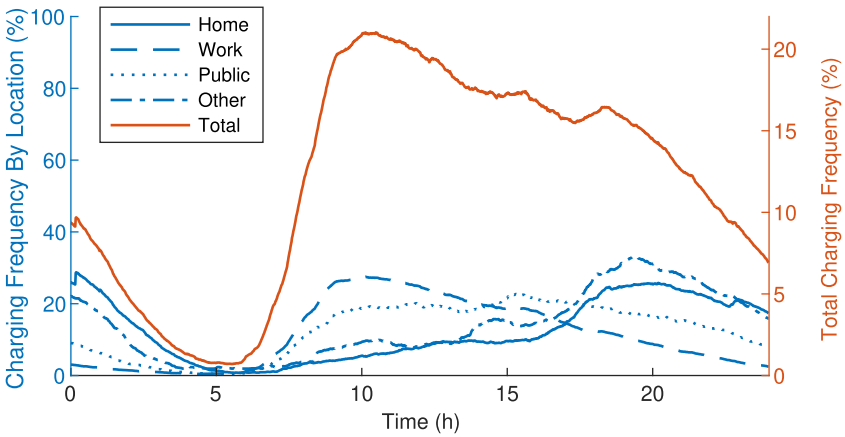

FIGURE 1 Daily variation in active charging events [27]

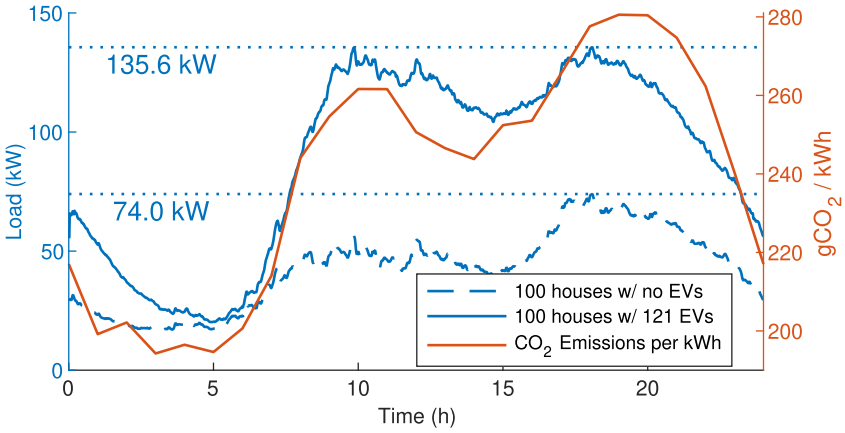

FIGURE 2 The average household in the UK has 1.21 vehicles. If all vehicles were electric, household load profile increases dramatically. EV, electric vehicles

2 | SYSTEM MODEL

The system model and its inputs are described as follows.

2.1 | EV charging, household load and CO_2 emissions

The charging behaviour of EVs is statistically quantified in [27], which gathers data from 31,765 EV trips and 16,229 charging events. With this data, a probability distribution for the expected number of active charging EVs throughout the day is constructed, as shown in Figure 1. The expected load per vehicle $P_{EV}(t)$ is then constructed for random uncoordinated charging.

The electric power demand of 251 selected households with and without electric heating in the UK is presented in [28]. Approximately 10% of households use electric heating [29]. With this data, the expected load per household $P_H(t)$ on a cold winter day is constructed.

The average number of vehicles per household was 1.21 in the UK, 2017 [30]. When EV and household load profiles are combined, as shown in Figure 2 for 100 households, the peak load increases to 83%. However, off-peak times are well matched.

MyGridGB [31] logs and analyses power production in real-time across Great Britain. With this data, hourly CO_2 emissions per kWh averaged over 30 days is shown Figure 2, which correlates strongly with loading patterns. Negating marginal carbon emissions, by charging an EV between 3 and 5 AM instead of 7–8 PM, CO_2 emissions are reduced to almost 30%. This demonstrates the huge potential for smart charging to reduce carbon emissions alongside the peak load.

2.2 | Power network

A distribution network of B buses is modelled as in [32]. The power demand $S_b[n] = P_b[n] + jQ_b[n]$, $j = \sqrt{-1}$ at each bus $b \in \boldsymbol{B} = \{1, 2, \ldots, B\}$ at time $t = n\Delta t$, $n \in \mathbb{Z}^+$ is defined

$$\left.\begin{aligned} P_b[n] &= H_b(P_H[n] + \eta_{EV} P_{EV}[n]) \\ Q_b[n] &= 0 \end{aligned}\right\} \quad \forall \; 0 \le n < \frac{24}{\Delta t} \tag{1}$$

H_b is the number of houses supplied at each bus b, η_{EV} is the network-wide EV penetration, P_H and P_{EV} are average expected household and EV charging load profiles per household and per EV, respectively. Perfect power factor correction is assumed at each bus, so the reactive power input

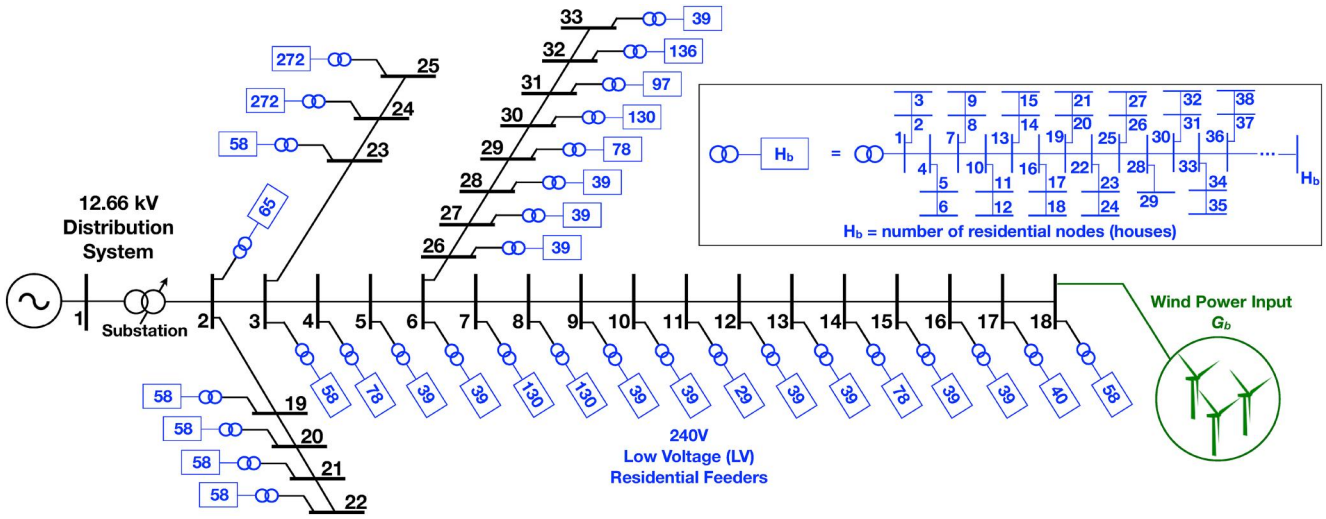

FIGURE 3 IEEE 33 bus 12.66 kV distribution network

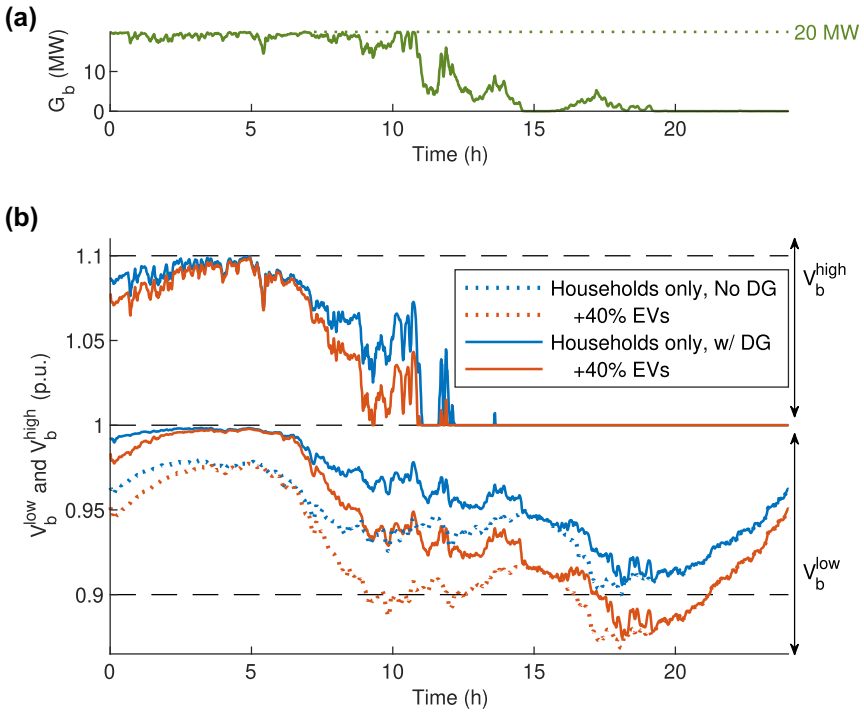

FIGURE 4 Adding distributed generation (DG) only increases volatility of voltage deviation. (a) G_b: DG wind power input at bus 18, (b) Maximum $\left(V_b^{\text{high}}\right)$ and minimum $\left(V_b^{\text{low}}\right)$ worst bus voltages

Q_b is negligible. Time interval $\Delta t = \frac{1}{60}$ (1 min). Power flow between sequential nodes $a, b, c \subset \boldsymbol{B}, a \neq b \neq c$ in the network is then defined by the Branch Flow Model [33].

$$\sum_{c=1}^{C} S_{b,c}[n] = S_{a,b}[n] - Z_{a,b}|I_{a,b}[n]|^2 - S_b[n] \quad (2)$$

$$V_b[n] - V_c[n] = Z_{b,c} I_{b,c}[n] \quad (3)$$

$$S_{b,c}[n] = V_b[n] I_{b,c}^*[n] \quad (4)$$

where $c \in [1, 2, \ldots C]$ are child nodes of node b, which is in turn child of a. Along branch $b \rightarrow c$: $S_{b,c} = P_{b,c} + jQ_{b,c}$ is the sending end complex power transfer, $I_{b,c}$ is the current phasor and $Z_{b,c} = R_{b,c} + jX_{b,c}$ is the line impedance. S_b is the net power drawn from bus b and V_b is the voltage phasor. This model allows complex power flow and voltage deviation at each link and bus to be calculated iteratively for each time step n.

This is simulated for the IEEE 33-bus 12.66 kV distribution network shown Figure 3, adapted from [34]. Each bus connects to a Low Voltage (LV) 240 V residential feeder with H_b households. The real power demand at each LV node

follows $P_H(t)$ and $P_{EV}(t)$. The line impedance in the LV feeders is negligible, that is the only reactive load is from capacitive and inductive effects on the 12.66 kV lines.

Expected load under 0% and with 40% EVs is applied for zero DG, and voltage deviation at each bus derived using Matpower [35]. The lowest bus voltage in the network V_b^{low} (regardless of which specific bus) is shown by dotted lines in Figure 4b. In European normal grid operations, voltage deviation at any bus should not exceed the statutory limit of 1 ± 0.1p.u. [36]; however, this range can be redefined without loss of generality. The number of houses (H_b) is chosen here such that this lower limit is reached under household load only. Thus the network can be considered to have zero EV Capacity under random uncoordinated charging. EVs bring V_b^{low} well outside of its acceptable range.

2.3 | Renewable DG

It is desirable to increase deployment of renewable DG due to various social, economic and environmental goals. However, excessive DG can cause overvoltage, thermal overloading of equipment and high-frequency distortions. To avoid this, DG curtailment is often necessary. To maximise return on investment in renewable systems, DG curtailment must be minimised.

DG is equivalent in the system to negative load. However, to differentiate from demand, power generation at bus b is denoted G_b. DG Capacity (a.k.a Hosting Capacity) is defined as the upper limit of DG beyond which overvoltage occurs [16, 37], that is V_b^{high} should not exceed 1.1 p.u.

Wind power generation profile is modelled using wind speed sensor readings gathered at 1s intervals over 172 days from an offshore wind farm in [38]. Power is derived using the Vestas V164-8.0 wind turbine power curve [39].

Problems of excessive DG are most noticeable when concentrated at end of long and lightly loaded feeders [40]. Figure 4 shows a 20 MW wind power profile input at bus 18. Maximum V_b^{high} and minimum V_b^{low} voltage deviations are shown in Figure 4b. All other bus voltages fall between V_b^{high} and V_b^{low}.

First, since V_b^{high} touches the upper limit 1.1 p.u., this is considered the DG Capacity of the unconstrained network. Second, voltage now spans the full range of its acceptable limits and minimum voltage remains unchanged. Unconstrained DG aggravates volatility since it is non-synchronised with consumer demand. This paper proposes two schemes to synergise DG and EV charging such that capacity of both is improved simultaneously.

2.4 | Control architecture

The proposed scheme uses the three-tier hierarchical network topology common in emerging Smart Grid and Internet of Things (IoT) environments [41], shown Figure 5. There are three node types:

1. *Central Control Unit (CCU):* This is the main network coordinator, for example the Distribution System Operator (DSO). It is connected via data link to Intermediary Control Units (ICUs) permeated throughout the network. It receives periodic status beacons from each ICU and based on these, transmits control instructions.
2. *Intermediary Control Unit (ICU):* These are mid-tier nodes which coordinate regionally co-located demand-response assets via Smart Devices (SDs). This alleviates computation load on the Central Control Unit (CCU) as well as traffic load on the ICT system [41]. Every update period, the ICU broadcasts 'Status Request' to its SDs and receives their replies. If a control signal from the CCU is received, actuation instructions are transmitted to relevant SDs. In this study there is one ICU_b for each distribution bus b, but in practice an ICU could exist anywhere, numerous demand-response assets must be managed.
3. *Smart Device (SD):* These are bottom-tier nodes that conduct measurements and/or actuations. Practically, they may be home or building Energy Management Systems

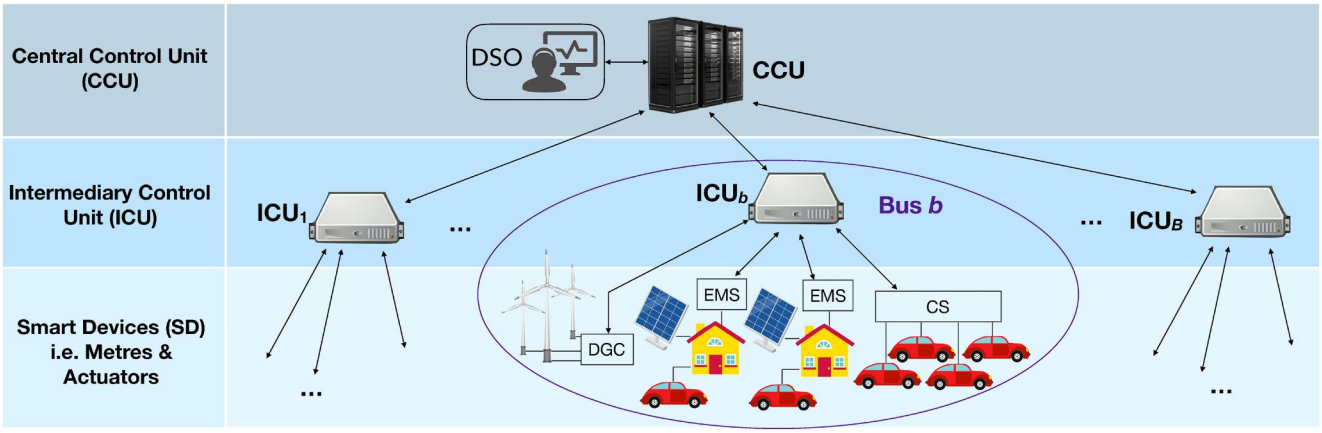

FIGURE 5 Three-tier hierarchical communications topology for the proposed Smart EV Charging scheme. CCU, central control unit; DGC, distributed generation controllers; EMS, energy management systems; ICU, intermediary control unit; SD, smart device

(EMSs), networked Charging Stations (CSs) and Distributed Generation Controllers (DGCs). These will be numerous and pervasive, so operation is kept simple. The SD receives control commands (e.g. curtailment limits) from its ICU, and replies with status messages. Upon receiving a curtailment limit, the SD ensures its overall power does not exceed this limit.

This architecture is in line with recent open smart charging and Demand-Response communications standards OpenADR (now IEC 62746-10-1) [42] and OCPP [43]. Upper-tier communication (CCU-ICU) can be achieved with OpenADR, where the CCU is Virtual Top Node (VTN) and ICUs are Virtual End Node (VEN) with PUSH protocol enabled. Status beacons are sent via EiReport service, and control commands via EiEvent. Lower-tier communication (ICU-SD) is also configured using OpenADR, however is easily extensible to any OCPP-ready device via External Smart Charging in OCPPv2.0. All SDs are VEN of the ICU. Curtailment limits are sent via OpenADR EiEvent, and status information via EiReport service.

Practical update interval is subject to two systematic constraints. First, ICT infrastructure represents large investment for a system as ubiquitous as the power network. Using a short update interval with fast sensor readings increases data volume and system traffic, which raises bandwidth requirements and cost of ICT hardware. A tradeoff ensues between granularity of control and cost of data collection.

Second, operating bodies in the power network are traditionally unaccustomed to latency-critical ICT applications, and update interval is far from homogenised across the industry. OCPP has scope for charging limit duration in seconds, as well as rapid demand-response times due to transaction and billing requirements; however, Supervisory Control and Data Acquisition (SCADA) is normally collected from wind turbines at 10 min intervals. Any control scheme is subject to the slowest interval available. There will inevitably be a transition period during which slower-than-desired update interval must be tolerated.

Latency can be reduced in the system, but this comes at a cost. Understanding key tradeoffs between practical update period and smart charging performance is vital.

3 | SCHEME I: SMART CURTAILMENT

Power infrastructure is normally sized according to peak load. By curtailing charging load and DG, peak load can be reduced. This achieves minimal power hardware replacement as EV & DG penetrations rise, reducing costs for the system operator.

To do this, load is categorised as flexible or non-flexible. Non-flexible load must be delivered on demand. Flexible load can tolerate a reasonable delay. Priority is decided by user input: 'High priority' users are non-flexible load, and 'low priority' flexible users are compensated for potential charging delay with cheaper energy prices. Conceivably, many users are willing to charge their EV overnight instead of early evening to save money. This renders the scheme economically viable.

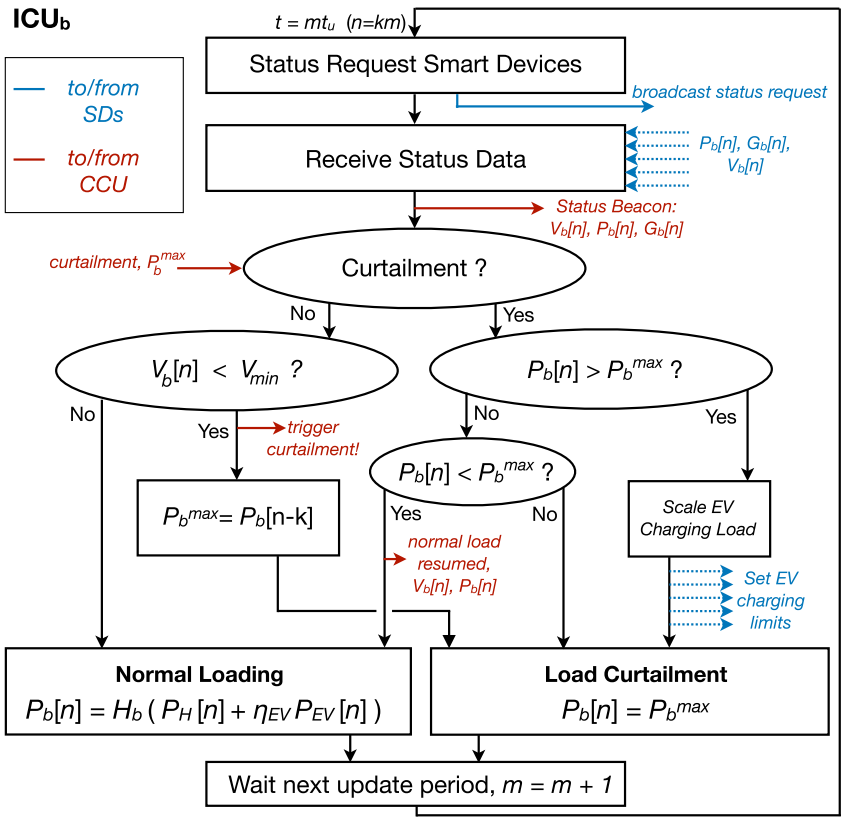

FIGURE 6 Smart EV Charging algorithm at ICU_b (*P*-CUR only). CCU, central control unit; ICU, intermediary control units; P-CUR, *P*-curtailment; SD, smart device

This paper treats household energy demand as non-flexible and all EV charging as flexible, although these definitions may be rearranged without loss of generality. It is assumed that the distribution network has been designed to accommodate all non-flexible load. Then only flexible load need be curtailed to keep voltage within bounds.

To prevent undervoltage, EV charging load is curtailed (*P*-curtailment, *P*-CUR). To prevent overvoltage, DG is curtailed (*G*-curtailment, *G*-CUR).

P-CUR for each ICU$_b$ is shown Figure 6. Every update interval mt_u, $t_u = k\Delta t$, $k, m \in \mathbb{Z}^+$, each ICU requests status information from its SDs to gather bus voltage $V_b[m]$, power demand $P_b[m]$ and DG input $G_b[m]$, and forwards this to the CCU. It also gathers available flexible load from each SD and stores this locally. The CCU then receives three status vectors every update interval

$$\vec{V}[m] = \begin{bmatrix} V_1[m] \\ \vdots \\ V_B[m] \end{bmatrix}, \vec{P}[m] = \begin{bmatrix} P_1[m] \\ \vdots \\ P_B[m] \end{bmatrix}, \vec{G}[m] = \begin{bmatrix} G_1[m] \\ \vdots \\ G_B[m] \end{bmatrix} \quad (5)$$

3.1 | *P*-curtailment

P-CUR is triggered at interval $m = m_P$ by any bus voltage below the limit $V_{\min}$. ICU$_b$ begins curtailment at bus b and notifies the CCU. Due to the radial topology of the distribution network, V_b^{low} is affected by load changes in any other bus. Therefore, all buses must curtail simultaneously, with maximum power corresponding to the last received power vector at CCU before the trigger.

$$\vec{P}^{\max}[m] = \begin{bmatrix} P_1^{\max}[m] \\ \vdots \\ P_B^{\max}[m] \end{bmatrix} = \begin{bmatrix} P_1[m_P - 1] \\ \vdots \\ P_B[m_P - 1] \end{bmatrix} = \vec{P}[m_P - 1] \quad (6)$$

The CCU then notifies each ICU$_b$ of its maximum power $P_b^{\max}$, which launches curtailment at every other bus.

During *P*-CUR, each ICU$_b$ repetitively updates the charging limits of all its connected flexible loads to ensure $P_b \le P_b^{\max}$. Non-flexible load is met by priority, and the remaining available power is distributed proportionally between all active charging EVs. This limits total network load to

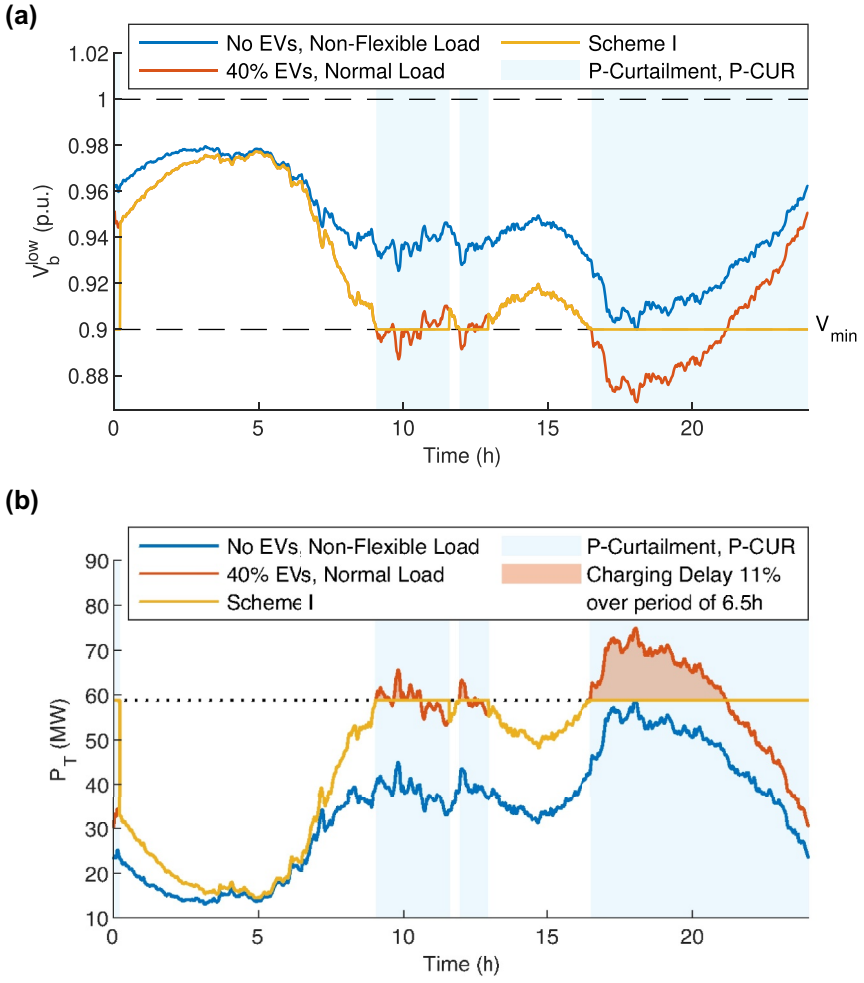

FIGURE 7 P -Curtailment only, Scheme I. (a) Minimum Bus Voltage, (b) P_T: Total Real Power Demand P-CUR, P-curtailmentI

$$P_T[m] = \sum_{b=1}^{B} P_b^{\max}[m] \tag{7}$$

And ensures V_b^{low} is limited to $V_{\min}$. Since the network is designed to meet non-flexible load requirements, it is always possible to reduce flexible load such that V_b^{low} is kept within bounds. The limit $P_b^{\max}$ is maintained until all delayed charging load is satisfied. At this point, ICU_b resumes normal load, notifying the CCU of its reduced power. This continues until all EV charging queues at all ICUs are empty.

V_b^{low} and P_T under *P*-CUR is shown Figure 7. Several Key Performance Indicators (KPIs) are visible:

- Voltage Control: Figure 7a. With no DG input, *P*-CUR ensures load is never large enough to bring V_b^{low} below statutory limits. Under zero latency, $P_b^{\max}$ can be instantly initiated in response to undervoltage, so perfect voltage control is achieved.
- *Peak Shaving:* Figure 7b. Curtailing flexible load subject to voltage conditions inherently reduces peak load in the system.
- *EV Charging Delay:* Curtailing charging load causes delays for subscribing EV owners during peak hours. Delay is incurred only when unconstrained load exceeds curtailed load. This delay period is shown in shaded orange, Figure 7b. Daily charging delay is the ratio of mean normal to curtailed load during this period, in this case 11% over 6.5 h. An EV charging during these peak hours takes on average 11% longer to gain the same amount of charge.
- CO_2 *Emissions:* Daily carbon emissions are calculated assuming all non-DG power input follows emissions from Figure 2. Since *P*-CUR reschedules charging load from peak

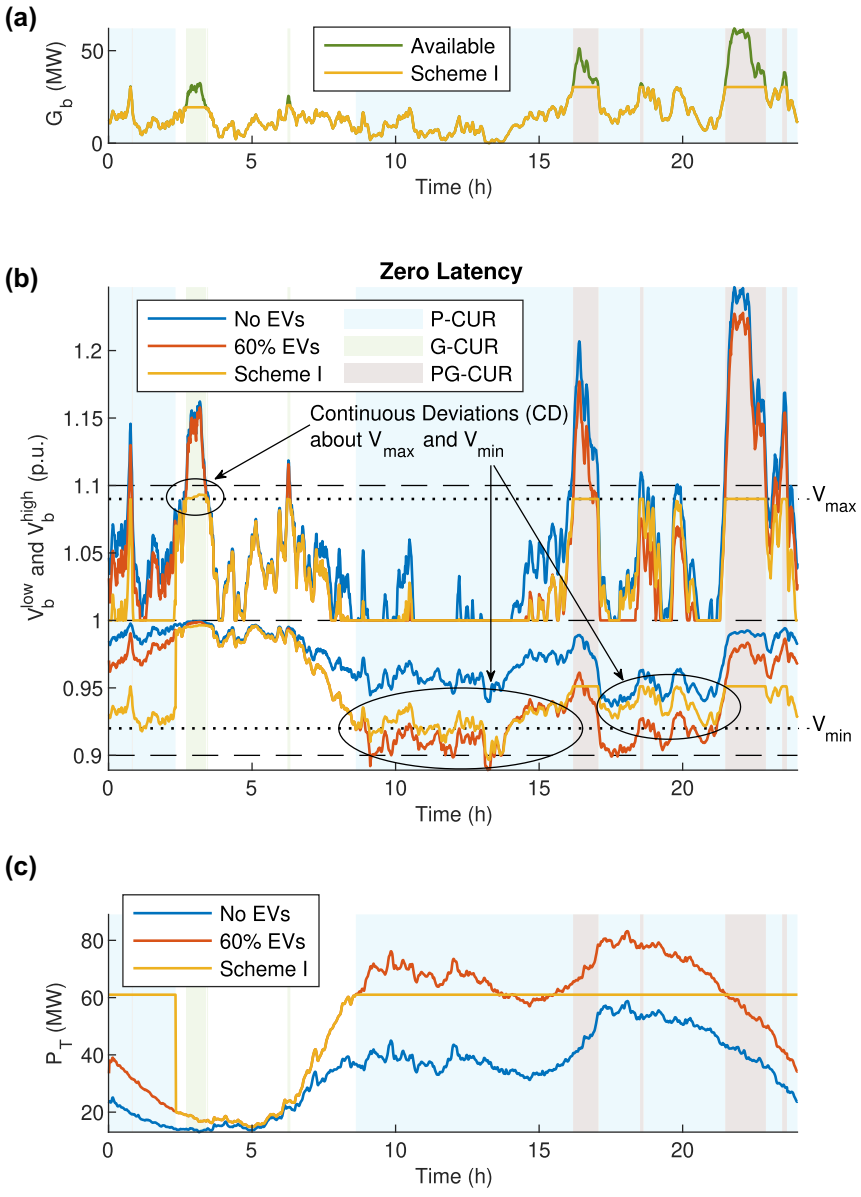

FIGURE 8 Zero Latency, Scheme I (a) G_b: DG wind power profile at bus 18, (b) $V_b^{\text{high}} V_b^{\text{low}}$: Upper & Lower Worst Bus Voltages, (c) P_T: Total Real Power Demand. EV, electric vehicles; G-CUR, G-curtailment; P-CUR, P-curtailment; PG-CUR, PG-curtailment

hours to lower emission hours overnight, less CO_2 is emitted overall. This saving grows as η_{EV} increases.

- *EV Capacity:* Undervoltage is avoided, so EV Capacity has increased compared to the unconstrained system.

3.2 | *G*-curtailment

The same process can be used to curtail DG to avoid overvoltage. *G*-CUR is triggered at interval $m = m_G$ by any bus voltage above limit $V_{\max}$. Any ICU_b that detects overvoltage begins curtailment to the last received values at the CCU

$$\vec{G}^{\max}[m] = \begin{bmatrix} G_1^{\max}[m] \\ \vdots \\ G_B^{\max}[m] \end{bmatrix} = \begin{bmatrix} G_1[m_G - 1] \\ \vdots \\ G_B[m_G - 1] \end{bmatrix} = \vec{G}[m_G - 1] \quad (8)$$

Each ICU_b then issues generation limits to all subsidiary SDs, ensuring $G_b \le G_b^{\max}$. This limits total DG to

$$G_T[m] = \sum_{b=1}^{B} G_b^{\max}[m] \quad (9)$$

No DG storage is assumed. Thus, the limit $G_b^{\max}$ is maintained only while generation is available in excess.

V_b^{low}, V_b^{high}, G_T and P_T under Scheme I are shown in Figure 8 with 60 MW wind farm input at bus 18% and 60% EV penetration. Several observations can be made.

- Voltage Control: Figure 8b. Scheme I effectively contains voltage deviation between statutory limits. However, since there are now two inputs that determine bus voltage, $\vec{P}$ and $\vec{G}$, curtailment in either one leads to Continuous

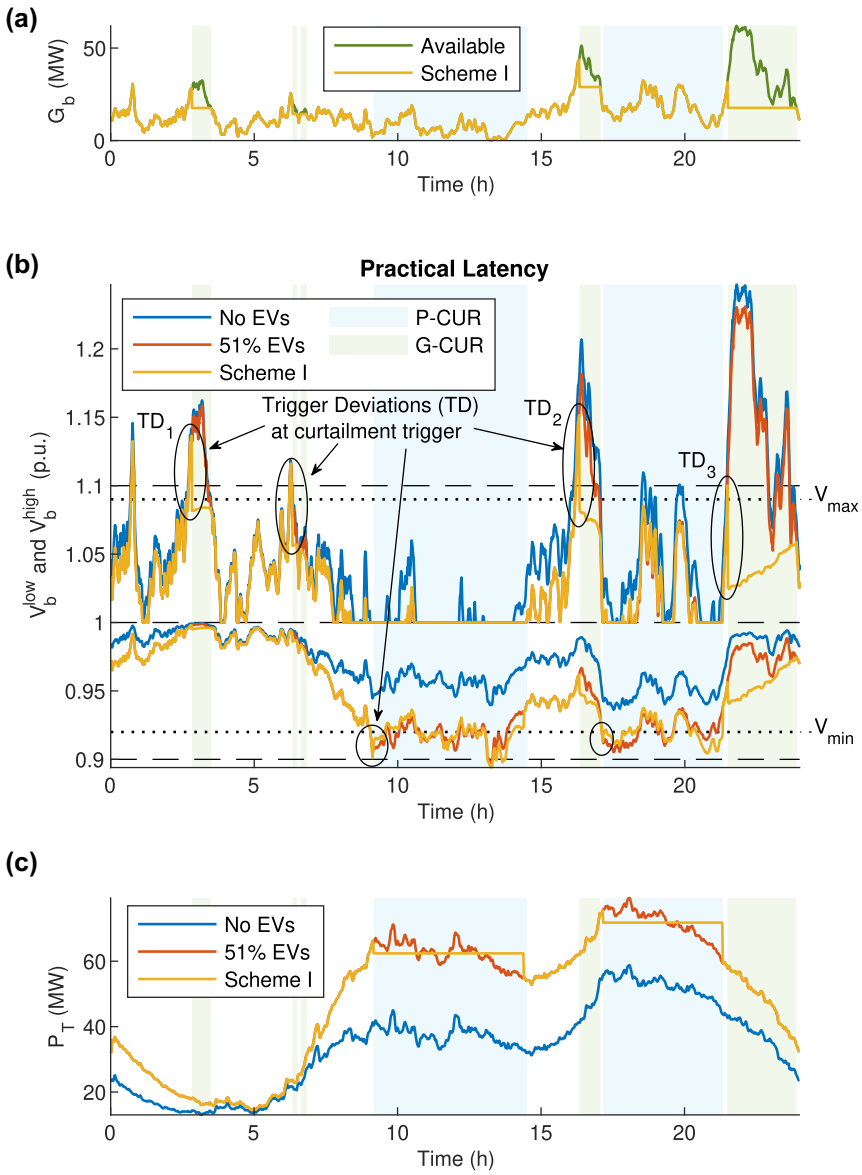

FIGURE 9 Practical Latency, t_u = 10$min, Scheme I (a) G_b: DG wind power input at bus 18, (b) $V_b^{\text{high}} V_b^{\text{low}}$: Upper & Lower Worst Bus Voltages, (c) P_T: Total Real Power Demand. EV, electric vehicles; G-CUR, G-curtailment; P-CUR, P-curtailment

Deviation (CD) about V_{min} or V_{max}. Variation in unconstrained P during G-CUR leads to CD about V_{max}. Unconstrained G during P-CUR leads to CD about V_{min}. During PG-curtailment (i.e. both P- and G-CUR simultaneously), there is no deviation as both are constant at their curtailed limits.

EV charging is spread throughout the network, whereas DG input is concentrated at a single bus. This, combined with the inherent volatility of renewable generation, means CD is much more prominent about V_{min} (during P-CUR) than about V_{max}.

- *User Inconvenience:* Figure 8b. To mitigate CD, the margin formed by V_{min} and V_{max} is adjusted away from statutory limits. However, this also means P_T and G_T must be curtailed at lower thresholds. For EVs, this means longer charging delays for subscribing users. For DG, this means lower average power output, reducing returns on investment in renewable systems.
- CO_2 *Emissions:* Greater DG penetration brings significantly reduced carbon emissions, since a higher proportion of total power input is renewable.
- *EV & DG Capacity:* Voltage stays within bounds despite rise in EV and DG penetration, reflecting capacity increase of both compared to the unconstrained system.

3.3 | Practical latency

Without perfect communications, sensor readings must be gathered with update period t_u, that is a delay up to t_u may follow over- or undervoltage before curtailment is triggered. Voltage deviations during this period are termed Trigger Deviations (TDs). Figure 9 shows Scheme I with $t_u = 10$ min.

- *Voltage Control:* Figure 9b. There is striking difference in magnitude between TD at V_{min} and V_{max}. For P-CUR, TD is comparable in size to CD. In contrast, TD for G-CUR is much

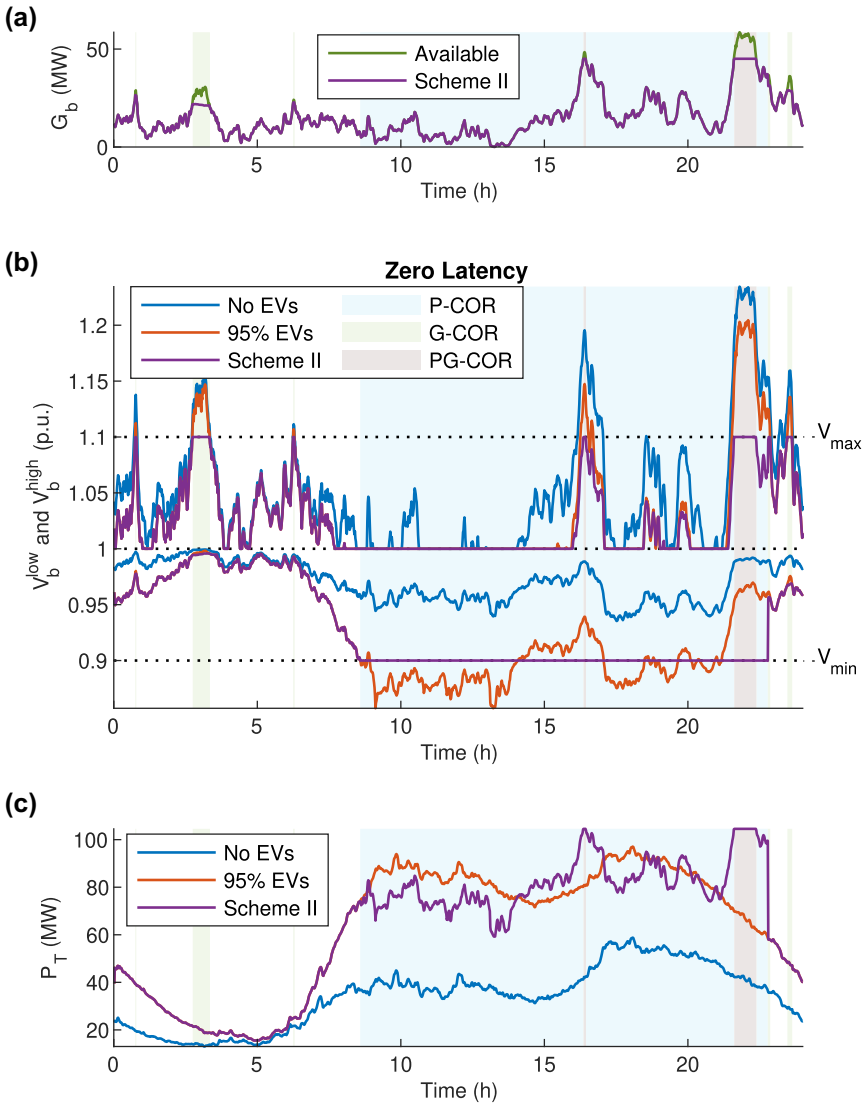

FIGURE 10 Scheme II under Zero Latency (a) G_b: DG wind power input at bus 18, (b) V_b^{high} V_b^{low}: Upper & Lower Worst Bus Voltages, (c) P_T: Total Real Power Demand. EV, electric vehicles; G-COR, G-correction; P-COR, P-correction; PG-COR, PG-correction

larger. The amount exceeded in both depends on unconstrained variation during the trigger delay, so has stochastic magnitude.

- *Peak Shaving:* TD is also visible in the DG and load profiles, Figure 9a and 9c. At each curtailment trigger, $\overline{P}$ and/or $\overline{G}$ are allowed to deviate freely before curtailment, leading to spikes above the curtailment limit. Power equipment is sized according to peak values, so it is desirable to limit this spike.
- *User Inconvenience:* Curtailment limits now depend on where the system was t_u minutes prior to the trigger. This leads to a stochastic limit, where G_T may be high (Figure 9b: TD_1, TD_2) or low (TD_3). Statistically, this effect tends towards overcurtailment: P_T and G_T are on average lower than is required. This increases EV charging delay and decreases DG energy input.

4 | SCHEME II: SMART CORRECTION

By relaxing peak shaving requirements, Scheme II maximises power transfer when it is cheap, that is during non-peak times or when renewable generation is high. Scheme II uses the same ICT framework from Section 2.4, with curtailment triggered in response to over- or under-voltage at any bus. However, curtailment limits in Scheme II are corrected every update interval to optimise power flow.

Bus voltages are some function f of load and DG vectors

$$\vec{V}[n] = f\left(\vec{P}[n], \vec{G}[n]\right) \tag{10}$$

where f depends on static characteristics such as number of buses, topology, line impedances, etc. Assuming small changes in Δt, this can be sequentially approximated via first order Taylor series

$$\vec{V}[n] = \vec{V}[n-1] + \boldsymbol{J}_f[n-1]\left(\Delta\vec{P}[n] - \Delta\vec{G}[n]\right) \tag{11}$$

$$\Delta\vec{P}[n] = \vec{P}[n] - \vec{P}[n-1] \tag{12}$$

$$\Delta\vec{G}[n] = \vec{G}[n] - \vec{G}[n-1] \tag{13}$$

where $\boldsymbol{J}_f[n-1]$ is the Jacobian evaluated at $\vec{V}[n-1]$

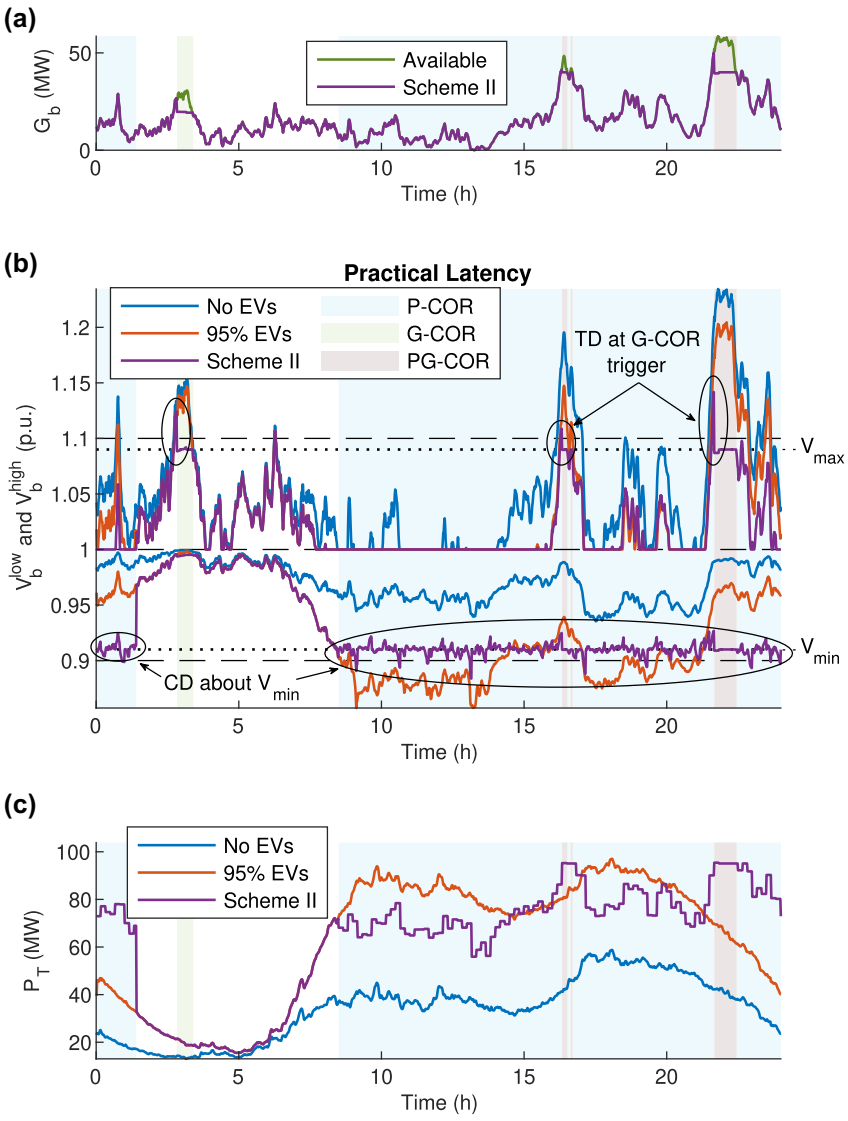

FIGURE 11 Scheme II under Practical Latency, $t_u = 10$\$min (a) G_b: DG wind power input at bus 18, (b) $V_b^{high} V_b^{low}$: Upper & Lower Worst Bus Voltages, (c) P_T: Total Real Power Demand. EV, electric vehicles; G-COR, G-correction; P-COR, P-correction; PG-COR, PG-correction

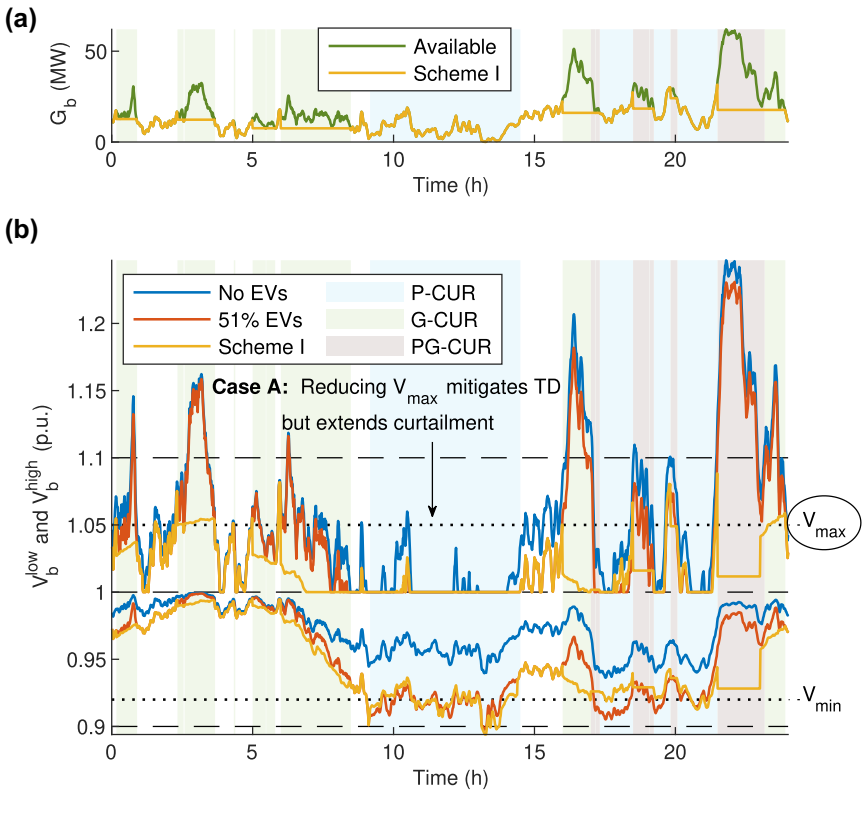

FIGURE 12 **Case A:** reducing V_{max} can mitigate trigger deviations (TD), but extends curtailment (shaded regions) and increases user inconvenience (a) G_b: DG wind power input at bus 18, (b) $V_b^{high}V_b^{low}$: Upper & Lower Worst Bus Voltages. EV, electric vehicles; G-CUR, G-curtailment; P-CUR, P-curtailment; PG-CUR, PG-curtailment

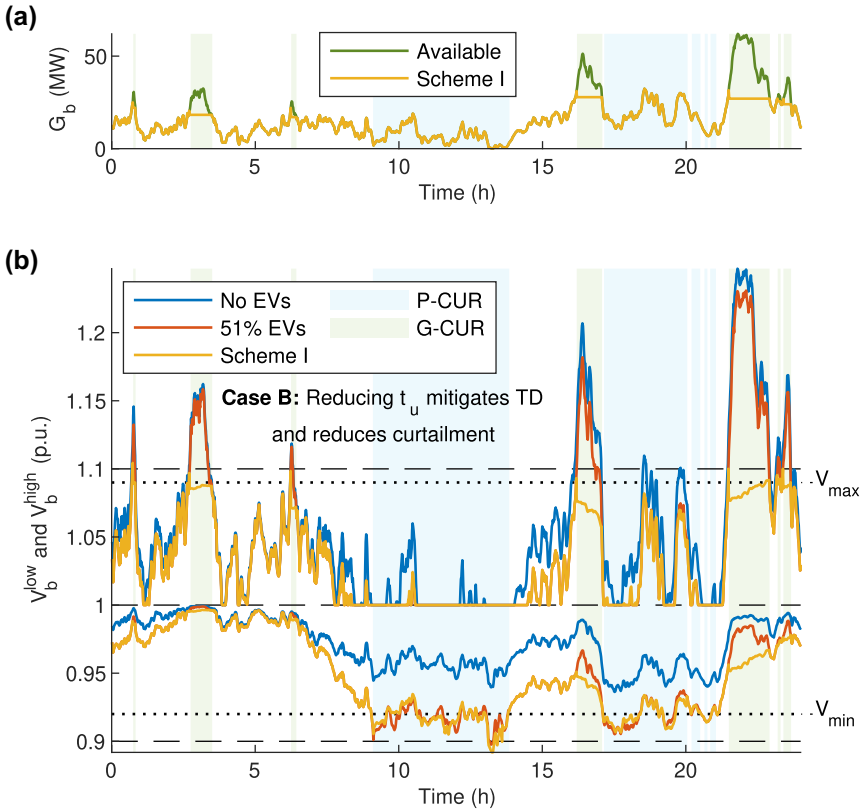

FIGURE 13 **Case B:** reducing t_u can mitigate trigger deviations (TD) and reduce curtailment (compare shaded regions with Figure 12) (a) G_b: DG wind power input at bus 18, (b) $V_b^{high}V_b^{low}$: Upper & Lower Worst Bus Voltages. EV, electric vehicles; G-CUR, G-curtailment; P-CUR, P-curtailment; PG-CUR, PG-curtailment

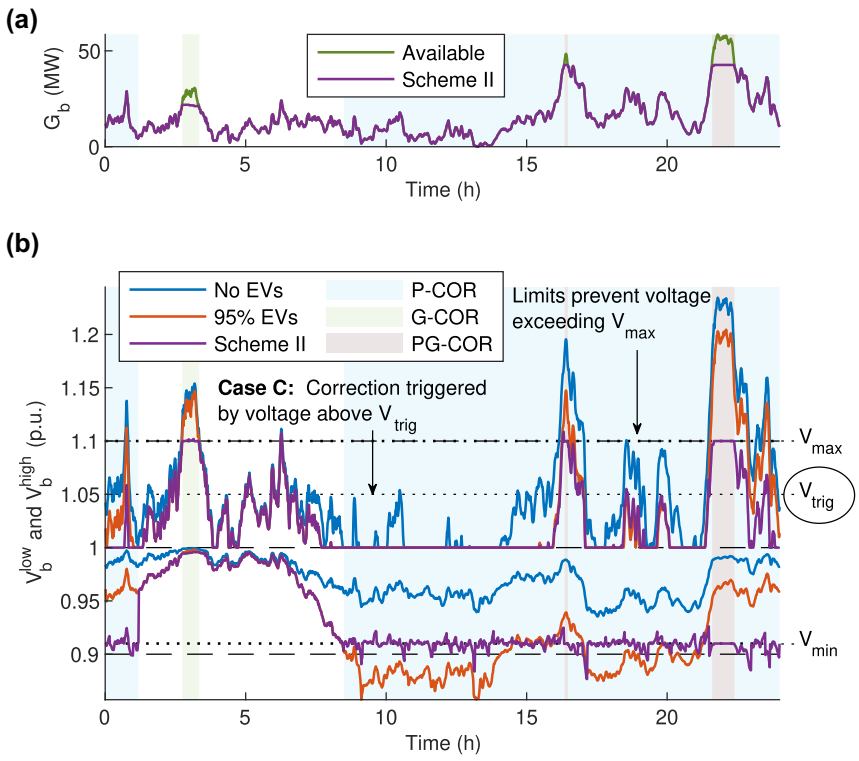

FIGURE 14 **Case C:** separating the trigger margin V_{trig} from continuous margin $V_{\max}$ effectively limits trigger deviations (TD) without extending curtailment (a) G_b: DG wind power input at bus 18, (b) V_b^{high}, V_b^{low}: Upper & Lower Worst Bus Voltages. G-COR, G-correction; P-COR, P-correction; PG-COR, PG-correction

TABLE 1 Six subschemes for voltage control in Exp. 1

	Subscheme	$V_{\min}$	$V_{\max}$	V_{trig}
Scheme I	(i)	0.9	1.1	-
	(ii)	0.92	1.095	-
	(iii)	0.93	1.09	-
Scheme II	(i)	0.9	1.1	1.04
	(ii)	0.92	1.095	1.03
	(iii)	0.93	1.09	1.02

$$\boldsymbol{J}_f[n-1] = \left[\begin{matrix} \frac{\delta V_1}{\delta P_1} & \frac{\delta V_1}{\delta P_2} & \cdots & \frac{\delta V_1}{\delta P_B} \\ \frac{\delta V_2}{\delta P_1} & \frac{\delta V_2}{\delta P_2} & \cdots & \frac{\delta V_2}{\delta P_B} \\ \vdots & \vdots & & \vdots \\ \frac{\delta V_B}{\delta P_1} & \frac{\delta V_B}{\delta P_2} & \cdots & \frac{\delta V_B}{\delta P_B} \end{matrix}\right]\Bigg|_{\vec{V}[n-1]} \tag{14}$$

To correct voltage conditions in the network, a change $\Delta\vec{P}$ can tailor a desired voltage vector $\vec{V}$ based on sensor readings of $\vec{V}[m]$ and $\Delta\vec{G}[m]$. Using Equation (11), this is

$$\Delta\vec{P} = \boldsymbol{J}_f^{-1}[m]\left(\vec{V}' - \vec{V}[m] + \boldsymbol{J}_f[m]\Delta\vec{G} - [m]\right) \tag{15}$$

The matrix $\boldsymbol{J}_f[m]$ can be computed in the interval $(m-1) < n < m$ by temporarily changing $P_b^{\max}$ at each bus by a small increment and noting the small change in $\vec{V}[n]$.

How to optimally allocate $\Delta\vec{P}$ and $\vec{V}$ is flexible to various power allocation algorithms. Computational effort is a strong concern. Equation 15 involves complex $B \times B$ matrix operations which can become overly intensive for large B. Fairness is another. Simply maximising $\sum_{b=1}^{B} P_b^{\max}$ during curtailment may lead to disproportionate power concentration at specific low-sensitivity buses, with large charging queues occurring elsewhere in the network. Scheme II achieves both computational savings and user fairness.

4.1 | *P*-correction

If only undervoltage is detected, only EV charging is curtailed and DG is unconstrained. During *P*-correction (*P*-COR), $\vec{P}^{\max}$ is adjusted every update interval by correction vector $\Delta\vec{P}^{\max}$.

$$\vec{P}^{\max}[m] = \vec{P}^{\max}[m-1] + \Delta\vec{P}^{\max} \tag{16}$$

$\Delta\vec{P}^{\max}$ must maximise overall power delivery incumbent to variable DG, while keeping all $\vec{V}$ within bounds. Fairness must

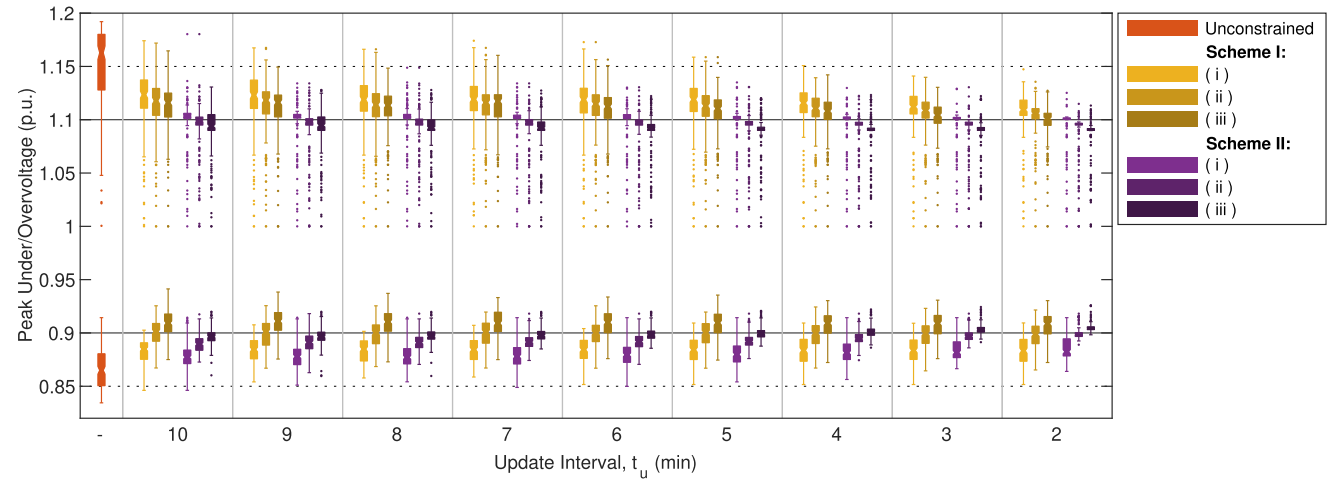

(a) Daily peak maximum and minimum voltage.

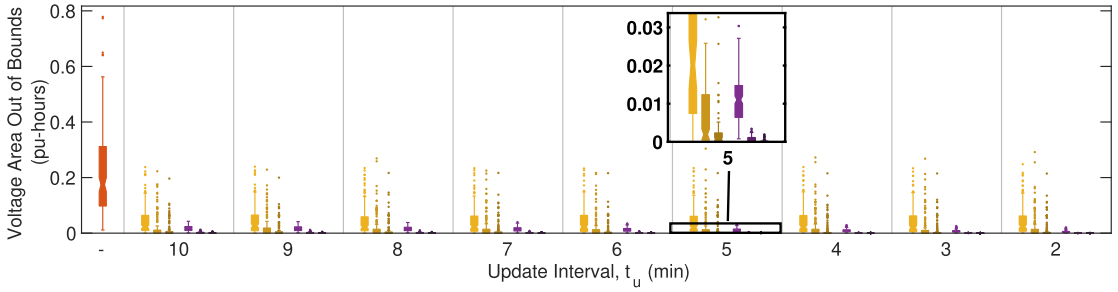

(b) Voltage area out of bounds.

FIGURE 15 Voltage effects of the six test systems in Exp. 1, shown Table 1

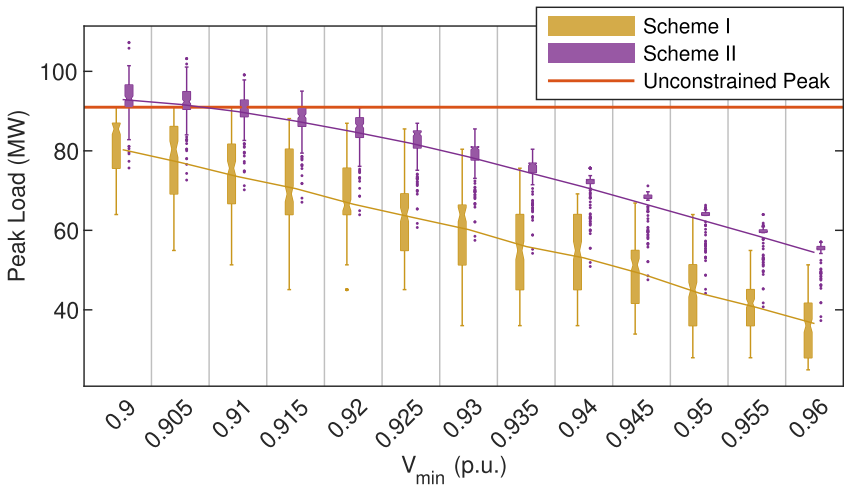

FIGURE 16 Peak Shaving performance of Scheme I and II

also be maintained, distributing available power evenly between buses. To do this, a fairness condition enforces that $\Delta P_T = \sum \Delta P_b^{\max}$ is implemented proportionally on each bus

$$\Delta \vec{P}^{\max} = \begin{bmatrix} k_1 \\ \vdots \\ k_B \end{bmatrix} \Delta P_T, \quad \sum_{k=1}^{B} k_b = 1 \tag{17}$$

where k_b are constants proportional to power demand at each bus on the trigger m_P. Load correction is then formulated.

$$\max \quad \Delta P_T \tag{18a}$$

$$\text{s. t.} \quad \vec{V}[m] \geq V_{\min} \tag{18b}$$

This is achieved by reformulating Equations (10) and (11)

$$\vec{V}[m] = f\left(P_T[m], \vec{G}[m]\right) \tag{19}$$

$$\vec{V}' = \vec{V}[m] + \boldsymbol{J}_{P_T}[m]\Delta P_T - \boldsymbol{J}_f[m]\Delta\vec{G}[m] \tag{20}$$

where $\boldsymbol{J}_{P_T}$ is drawn from $\boldsymbol{J}_f$ via weighted row addition

$$\boldsymbol{J}_{P_T}[m] = \left[\begin{matrix} \frac{\delta V_1}{\delta P_T} \\ \vdots \\ \frac{\delta V_B}{\delta P_T} \end{matrix}\right]\Bigg|_{\vec{V}[m]} \left[\begin{matrix} \sum_{b=1}^{B} k_b \frac{\delta V_1}{\delta P_b} \\ \vdots \\ \sum_{b=1}^{B} k_b \frac{\delta V_B}{\delta P_b} \end{matrix}\right]\Bigg|_{\vec{V}[m]} \tag{21}$$

Using $\boldsymbol{J}_{P_T}$ eliminates the $B \times B$ matrix inverse from Equation (15), significantly reducing required computations.

The maximum in Equation (18a) occurs when $V_b^{\text{low}} = V_{\min}$. Which bus to choose for V_b^{low} is important, since ΔP_T should not bring another bus voltage out of bounds. From Equation (20), change ΔP_{T_b} can be calculated bringing each $V_b[m]$ to $V_{\min}$

$$\left[\begin{matrix} \Delta P_{T_1} \\ \vdots \\ \Delta P_{T_B} \end{matrix}\right] = \left[\begin{matrix} \frac{V_{\min} - V_1[m] + \sum_{b=1}^{B} \frac{\delta V_1}{\delta P_b}\Big|_{\vec{V}[m]} \Delta G_b[n]}{\frac{\delta V_1}{\delta P_T}\Big|_{\vec{V}[m]}} \\ \vdots \\ \frac{V_{\min} - V_B[m] + \sum_{b=1}^{B} \frac{\delta V_B}{\delta P_b}\Big|_{\vec{V}[m]} \Delta G_b[m]}{\frac{\delta V_B}{\delta P_T}\Big|_{\vec{V}[m]}} \end{matrix}\right] \tag{22}$$

The optimum is then the smallest (most negative) correction

$$\Delta P_T = \min_b \left[\Delta P_{T_1}, \ldots, \Delta P_{T_B}\right] \tag{23}$$

This ensures the new V_b^{low} is always $V_{\min}$.

These calculations are performed at the CCU every update interval during P-COR based on inputs $\vec{V}[m], \vec{G}[m]$ received from the ICUs. Changes $k_b\Delta P_T$ are then sent out to each ICU_b individually, who distribute this between their connected SDs.

If any ICU_b has insufficient EVs to meet its power limit, V_b^{low} will rise above $V_{\min}$, so voltage stays within bounds. The reduced P_b is sent to CCU on the next update interval, and $[k_1, \ldots, k_B]$ updated such that power limits at remaining buses can increase. Therefore the scheme is robust to non-uniform loading patterns and corrective within one iteration phase.

4.2 | *G*-correction

If only overvoltage occurs, only DG is curtailed and EV charging is unconstrained. During G-correction (G-COR), $\vec{G}^{\max}$ is corrected every update interval by change $\Delta\vec{G}^{\max}$

$$\vec{G}^{\max}[m] = \vec{G}^{\max}[m-1] + \Delta\vec{G}^{\max} \tag{24}$$

To do this, Equations (10) and (11) are reformulated

$$\vec{V}[m] = f\left(\vec{P}[m], G_T[m]\right) \tag{25}$$

$$\vec{V}' = \vec{V}[m] + \boldsymbol{J}_f[m]\Delta\vec{P}[m] + \boldsymbol{J}_{G_T}[m]\Delta G_T \tag{26}$$

where $\boldsymbol{J}_{G_T}$ is again drawn from $\boldsymbol{J}_f$

$$\boldsymbol{J}_{G_T}[m] = \left[\begin{matrix} \frac{\delta V_1}{\delta G_T} \\ \vdots \\ \frac{\delta V_B}{\delta G_T} \end{matrix}\right]\Bigg|_{\vec{V}[m]} \left[\begin{matrix} -\sum_{b=1}^{B} l_b \frac{\delta V_1}{\delta P_b} \\ \vdots \\ -\sum_{b=1}^{B} l_b \frac{\delta V_B}{\delta P_b} \end{matrix}\right]\Bigg|_{\vec{V}[m]} \tag{27}$$

and fairness condition is enforced

$$\Delta\vec{G}^{\max} = \left[\begin{matrix} l_1 \\ \vdots \\ l_B \end{matrix}\right]\Delta G_T, \quad \sum_{l=1}^{B} l_b = 1 \tag{28}$$

with constants l_b proportional to available power generation at each bus on trigger m_G. DG correction is then formulated.

$$\max \qquad \Delta G_T \tag{29a}$$

$$\text{s. t.} \qquad \vec{V}[m] \le V_{\max} \tag{29b}$$

This maximum occurs when $V_b^{\text{high}} = V_{\max}$. To do this, the change ΔG_{T_b} is calculated to bring each $V_b[m]$ to $V_{\max}$

$$\left[\begin{matrix} \Delta G_{T_1} \\ \vdots \\ \Delta G_{T_B} \end{matrix}\right] = \left[\begin{matrix} \frac{V_{\max} - V_1[m] - \sum_{b=1}^{B} \frac{\delta V_1}{\delta P_b}\Big|_{\vec{V}[m]} \Delta P_b[n]}{\frac{\delta V_1}{\delta G_T}\Big|_{\vec{V}[m]}} \\ \vdots \\ \frac{V_{\max} - V_B[m] - \sum_{b=1}^{B} \frac{\delta V_B}{\delta P_b}\Big|_{\vec{V}[m]} \Delta P_b[m]}{\frac{\delta V_B}{\delta G_T}\Big|_{\vec{V}[m]}} \end{matrix}\right] \tag{30}$$

and choosing the minimum (most negative) correction ensures the new V_b^{high} is always $V_{\max}$

$$\Delta G_T = \min_b \left[\Delta G_{T_1}, \ldots, \Delta G_{T_B}\right] \tag{31}$$

If DG at any bus falls below its limit, V_b^{high} drops below $V_{\max}$, so voltage stays within bounds. The reduced G_b is sent to the CCU on the next update interval and $[l_1, \ldots, l_B]$ updated so limits at remaining buses can increase.

4.3 | *PG*-correction (*PG*-COR)

If both $\vec{P}$ and $\vec{G}$ increase simultaneously, eventually $\vec{V}$ spans the full breadth of technical limits. In this case, both charging load and DG must be curtailed simultaneously.

This is formulated by simultaneous corrections, where bus a is corrected to $V_{\max}$ and bus b is corrected to $V_{\min}$

$$\begin{cases} \overset{a,b}{\Delta G_T} = \dfrac{V_{\max} - V_a[m] - \dfrac{\delta V_a}{\delta P_T}\overset{a,b}{\Delta P_T}[m]}{\dfrac{\delta V_a}{\delta G_T}} \\ \overset{a,b}{\Delta P_T} = \dfrac{V_{\min} - V_b[m] - \dfrac{\delta V_b}{\delta G_T}\overset{a,b}{\Delta G_T}[m]}{\dfrac{\delta V_b}{\delta P_T}} \end{cases} \tag{32}$$

These can be solved by substitution for any paired buses (a, b)

$$\overset{a,b}{\Delta P_T}[m] = \frac{\frac{\delta V_b}{\delta G_T}(V_{\max} - V_a) - \frac{\delta V_a}{\delta G_T}(V_{\min} - V_b)}{\frac{\delta V_a}{\delta P_T}\frac{\delta V_b}{\delta G_T} - \frac{\delta V_a}{\delta G_T}\frac{\delta V_b}{\delta P_T}} \tag{33}$$

A $B \times B \times 2$ correction matrix is then computed

$$\mathbf{\Delta} = \begin{bmatrix} \infty, \infty & \overset{1,2}{\Delta P_T}, \overset{1,2}{\Delta G_T} & \ldots & \overset{1,B}{\Delta P_T}, \overset{1,B}{\Delta G_T} \\ \overset{2,1}{\Delta P_T}, \overset{2,1}{\Delta G_T} & \infty, \infty & \ldots & \overset{2,B}{\Delta P_T}, \overset{2,B}{\Delta G_T} \\ \vdots & \vdots & & \vdots \\ \overset{B,1}{\Delta P_T}, \overset{B,1}{\Delta G_T} & \overset{B,2}{\Delta P_T}, \overset{B,2}{\Delta G_T} & \ldots & \infty, \infty \end{bmatrix} \tag{34}$$

Choosing the smallest magnitude change ensures correction is made such that the new V_b^{high}, V_b^{low} are always $V_{\max}$, $V_{\min}$

$$(\Delta P_T, \Delta G_T) = \min_{a,b}[|\mathbf{\Delta}|], \tag{35}$$

where $|\mathbf{\Delta}|$ denotes absolute value of all matrix elements.

4.4 | Zero latency

Under zero latency, corrections can be applied instantly in response to voltage events. Figure 10 shows Scheme II under 60 MW DG input.

- Voltage Control: Figure 10b. During *P*-COR, any change in DG is reflected in ΔP_T such that V_b^{low} stays rigid at $V_{\min}$. Similarly, during *G*-COR, any load change is reflected in ΔG_T such that V_b^{high} is rigid at $V_{\max}$. All unacceptable voltage deviation is removed.
- *User Inconvenience:* The maximum available charging load and DG is used at any time, while keeping voltage within bounds. This minimises EV charging delay and maximises renewable power input, alleviating user inconvenience.
- *Peak Shaving:* Figures 10a and 10c. Peak load and peak DG tend to coincide. Peak load may rise above that of random uncoordinated charging, which was impossible under Scheme I.
- CO_2 *Emissions:* DG curtailment is minimised given voltage constraints, so CO_2 emissions are also.
- *EV & DG Capacity: G*-COR prevents overvoltage from excessive DG by adjusting generation limit according to load. Similarly, *P*-COR prevents undervoltage from excessive EV penetration. As a result, EV and DG penetrations can be increased to very high levels without voltage deviations out of bounds.

4.5 | Practical latency

Under practical latency, corrections can only be made with update period t_u. Figure 11 shows Scheme II for t_u = 10 min.

- *Voltage Control:* Figure 11b. CD is significantly restricted compared to Scheme I, since repetitive correction brings V_b^{low} to $V_{\min}$ or V_b^{high} to $V_{\max}$ every t_u. TD is prominent at the *G*-COR trigger.
- *Peak Shaving:* Figure 11c. TD is no longer visible in the load profile, since it is negligible compared to corrective load changes. This means peak load is under direct control of the CCU.
- *User Inconvenience:* Figure 11b. To mitigate CD, the margin formed by $V_{\min}$, $V_{\max}$ is adjusted. This reduces curtailment limits, meaning EV charging delays are extended and DG power input is reduced.

5 | CASE STUDIES

Four variables determine the performance of voltage control under practical latency: $V_{\min}$, $V_{\max}$, t_u and V_{trig}. The first three are common to Schemes I and II. The latter, V_{trig}, is specific to Scheme II. A case study of each is provided in turn.

5.1 | Case A: continuous margin (V_{min}, V_{max})

Figures 8, 9b and 11b showed that adjusting the limits (V_{min}, V_{max}) is necessary to mitigate CD. However, overvoltage due to TD was still prominent. In both schemes, reducing V_{max} further limits the TD spike. This is shown Figure 12 for Scheme I, where V_{max} is reduced to 1.05 pu. A similar graph can be drawn for Scheme II.

The disadvantage of this strategy is that it also significantly reduces the DG curtailment limit, leading to lower DG energy input. Further, reduced DG leads to lower voltages in the network overall. This means *P*-CUR (or *P*-COR for Scheme II) is also triggered earlier and at lower power, and EV charging delays are increased. Any reduction in the continuous margin formed by (V_{min}, V_{max}) significantly increases user inconvenience.

5.2 | Case B: Update interval (t_u)

Latency effects can also be mitigated by reducing the update interval t_u. This reduces the probability of a strong voltage deviation in between control intervals, shrinking TD in Scheme I and both TD and CD in Scheme II. As t_u is reduced, performance approaches that of the zero latency system in each scheme.

Cases A and B are the only latency mitigation strategies available for Scheme I. For comparison, Figure 13 shows Scheme I for $t_u = 3$ min. Overvoltage is effectively eliminated. Further, the reduced Trigger Deviation (TD) spike improves peak shaving. Importantly, since limits are chosen at more recent values, overcurtailment is reduced and curtailment limits increase. This is visible by comparing the size of the shaded regions in Figures 12 and 13. Reducing t_u achieves improved voltage control without the cost to user inconvenience from Case A.

However, Case B also incurs a cost. Reducing t_u from 10 to 3 min triples the data volume in the underpinning ICT system. Hardware may need to be added or replaced to support the additional bandwidth and processing requirement, meaning deployment cost is increased. This represents a key performance-cost tradeoff between Cases A & B.

5.3 | Case C: Trigger margin (V_{trig})

Cases A and B are the only latency mitigation strategies available for Scheme I. However, Scheme II provides an additional parameter for voltage control. The voltage at which correction is triggered, V_{trig}, need not be the same as the limit to which voltage is corrected, V_{max}. *G*-COR with $V_{trig} < V_{max}$ allows corrective limits to anticipate overvoltage, avoiding TD without impeding on P_T and G_T.

This is shown in Figure 14. Any bus voltage above V_{trig} will trigger *G*-corrective limits, pre-empting a sudden peak in generation. This effectively reduces TD, and eliminates the user inconvenience drawbacks of Case A.

6 | SIMULATION

The performance of both schemes is consolidated statistically under 172 days of 1 s wind power input from [38]. This is to demonstrate that both schemes are rigorous to a variety of practical input profiles. The schemes are tested with 40 MW DG at bus 18%, and 80% EV penetration.

6.1 | Experiments

From Section 5, three cases of control strategy are available in Schemes I and II (Cases A–C). Effective voltage control requires these three cases to be appropriately balanced. Case A is unavoidable, but can be alleviated with Cases B and C. Further, Case A has knock-on effects to other KPIs. To demonstrate this, the simulation is run in two experiments:

- ***Exp. 1:*** To demonstrate effective balance of Cases A–C, six subschemes are tested, each with progressively severe voltage margins shown in Table 1 Each subscheme is simulated under 172 days of wind power profiles and t_u from 2 to 10 min.
- ***Exp. 2:*** To demonstrate knock-on effects, case A is tested in isolation. This is done in two parts:.
  a. V_{min} is incremented 0.9–0.96pu with V_{max} constant at 1.1pu.
  b. V_{max} is incremented 1.04–1.1pu with V_{min} constant at 0.9pu.

For each increment, the same 172 days of windpower profiles are simulated, $t_u = 10$ min and $V_{trig} = V_{max}$.

Experimental findings are evaluated separately for Voltage Control, Peak Shaving, User Inconvenience and CO_2 Emissions.

6.2 | Voltage control

Exp. 1. *Voltage control is assessed via peak daily values and voltage area out of bounds. These are shown in Figure 15 for each subscheme.*

- **Scheme I** *Case A*: Figure 15a. Peak undervoltage changes negligibly with t_u, since it is dominated by CD. The only recourse to this is increasing V_{min}, shown by the undervoltage improvement across (i)–(iii). *Case B*: Overvoltage is TD-dominated, and effectively reduced with t_u. Case B is therefore a compelling alternative to Case A for overvoltage control.
- **Scheme II** *Case A*: Figure 15b. Voltage deviation out of bounds is strongly reduced compared to Scheme I. This is due to the repetitive correction that brings (V_b^{low}, V_b^{high}) back to (V_{min}, V_{max}) every update interval. *Case B*: Figure 15a, t_u reduces both peak deviation as well as spread of peak values (seen from Inter-Quartile Range (IQR) in each box-whisker plot) above and below bounds. This

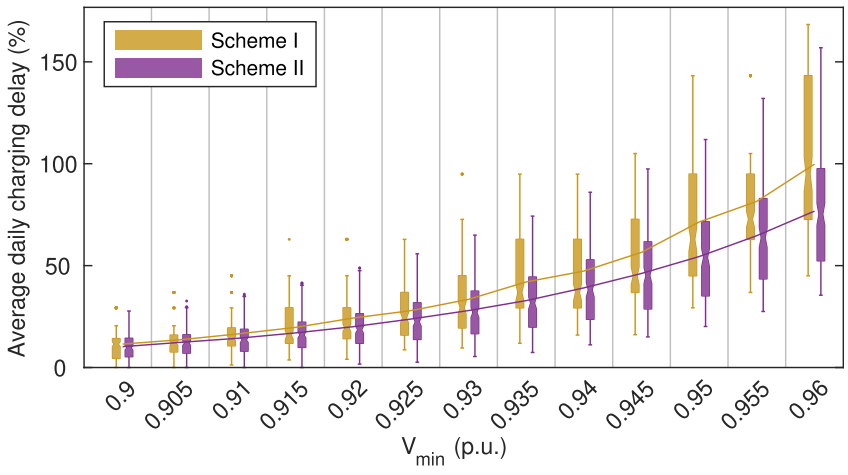

FIGURE 17 Average electric vehicle charging delay per user during peak hours

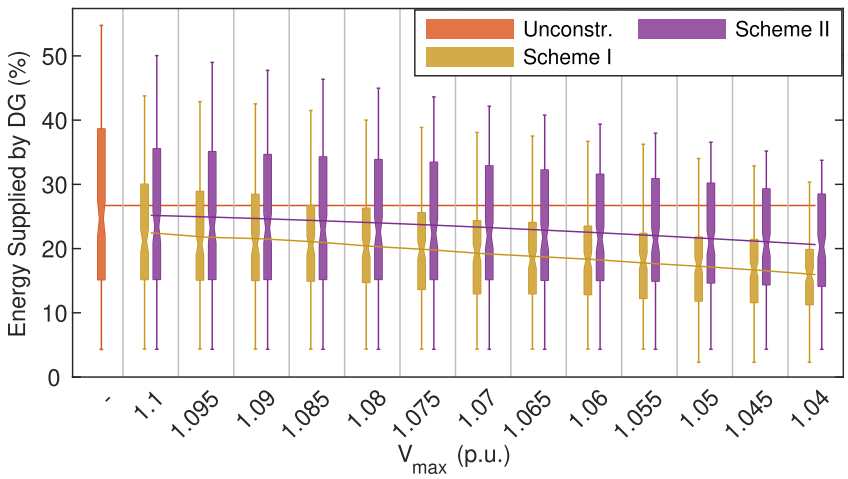

FIGURE 18 Daily Energy supply from renewable energy

delivers more predictable system response and allows for narrower control margins. *Case C*: The use of V_{trig} permits significant overvoltage improvement even at high t_u.

The spread of values in each box-whisker plot shows the statistical range of voltage deviations due to practical variation in wind availability. Deviations out of bounds are due to CD and/or TD resulting from practical latency constraints. Figure 15 shows that V_{min}, V_{max}, V_{trig} and t_u can be tweaked to achieve any desired voltage range.

6.3 | Peak shaving

Exp. 2a. V_{min} determines the EV charging curtailment limit and peak shaving performance. Peak load in both schemes is shown Figure 16.

By design, peak load in Scheme I is significantly less than the unconstrained system. In Scheme II, load scales with DG, which leads to significantly higher peak load. However, for practical $V_{\text{min}} > 0.915$pu, a consistent peak load decrease is maintained compared to unconstrained loading. Further, IQR in Scheme II is smaller, meaning equipment can be run closer to technical limits.

6.4 | User inconvenience

EV users require high power to charge their vehicles quickly, and investors in DG require high power to maximise returns. Curtailment therefore impedes on these objectives.

- *Charging Delay:* ***Exp. 2a.*** Average charging delay per EV during peak hours is shown Figure 17. Compared with Figure 16, this presents a key performance tradeoff: peak shaving must accompany increased charging delay. Further, peak load follows a linear downward trend, while charging delay rises exponentially.
- *DG Input:* ***Exp. 2b.*** A comparable effect is noticeable for DG, shown Figure 18. Both schemes curtail DG and reduce renewable energy supply. As V_{max} decreases, DG is curtailed more frequently and to a lower value, showing steady downward trend. However, Scheme II delivers consistently

FIGURE 19 Total daily carbon emissions

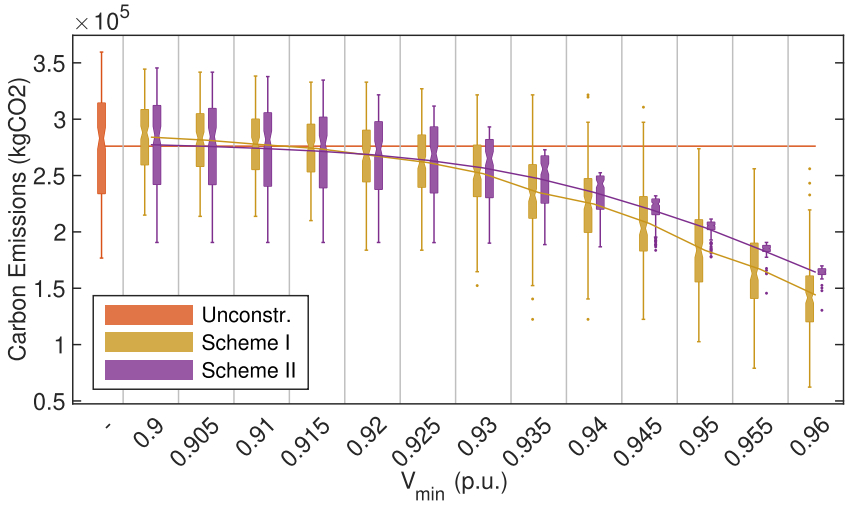

FIGURE 20 Mean daily CO_2 emissions

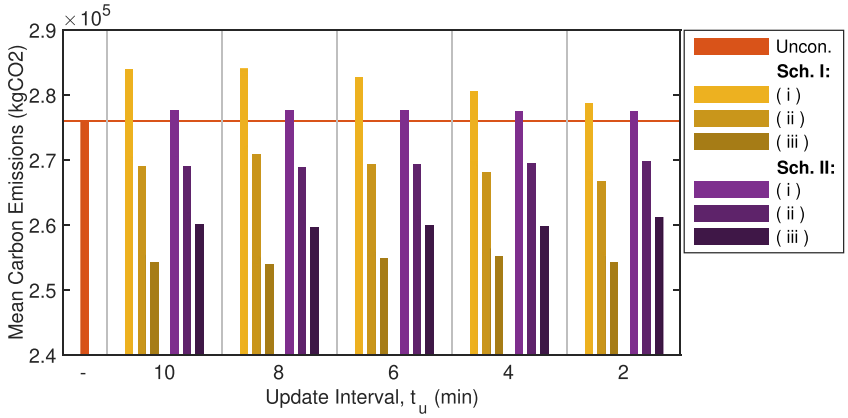

more renewable energy than Scheme I. Further, capability for case C means that Scheme II can use a higher V_{max} under the same overvoltage constraints.

6.5 | Carbon emissions

Exp. 2b. Curtailing DG reduces the proportion of renewable energy supply, which leads to a rise in CO_2 emissions. A graph can be drawn for this like Figure 18 but mirrored in the y-axis. As V_{max} falls, emissions rise.

Exp. 2a. However, Figure 2 showed that delaying charging load into off-peak hours overnight can significantly reduce emissions. Increasing V_{min} pushes more flexible load later into off-peak hours, therefore reducing carbon emissions, shown Figure 19.

Exp. 1. The net effect of these opposing relations for V_{min} and V_{max} is shown Figure 20 for the six subschemes in Table 1. As Case A grows more severe in both schemes (i)–(iii), emissions reduce from unconstrained values. This effect is homogenous across t_u. Therefore, both schemes effectively reduce CO_2 emissions at practical voltage margins in subschemes (ii)–(iii).

7 | CONCLUSION

Growing penetration of EVs and DG is driving sharper peaks in supply and demand. If poorly managed, these manifest as localised over- or undervoltage and disrupt service quality. Smart charging schemes address this by rescheduling EV charging load. How to do so while meeting the diverging needs of multiple concerned participants remains an open topic. This paper proposes two smart charging schemes for voltage control in the distribution network that can dramatically increase EV and DG capacity, and analyses the resulting key performance-cost tradeoffs.

Scheme I is optimised for peak shaving. This avoids extensive power hardware replacement as penetrations rise, cutting implementation and operating costs. Scheme II optimises cost-efficiency for subscribing users, that is EV owners and DG investors.

To support both schemes, a distributed control architecture is designed with multi-tier hierarchical topology. This minimises the computation load at the CCU and data traffic by offloading the coordination of demand-response assets onto regional ICUs. It is compatible with existing open communications standards such as OCPP and OpenADR. This reduces ICT hardware additions by harnessing the demand-response capability that is already rolled out across IP-connected

devices. Therefore the schemes are scalable and adaptable to a wide variety of network sizes and asset arrangements, and are readily applicable in the industrial environment.

Unconstrained EV and DG capacities are identified in the test system as 0% and 20 MW, respectively. Voltage control of both schemes for 80% and 40 MW is demonstrated in simulation under 172 days of wind power input, showing that the EV and DG capacity is dramatically improved. Further, key performance-cost tradeoffs in voltage control, peak shaving, user inconvenience, CO_2 emissions and ICT deployment are identified:

The first key tradeoff is between voltage control and peak shaving. Scheme II provides improved voltage control performance over Scheme I, particularly in overvoltage. In contrast, Scheme I displays a significantly lower peak load. However, critically, Scheme II achieves better voltage control under wide continuous voltage margins (Case A) and high update interval (Case B), which provides strong advantages in the other key tradeoffs. Peak load in Scheme II is also less variable, so equipment can be run closer to its limits.

The second key tradeoff is between peak shaving and user inconvenience. Scheme II has marked advantage in EV charging delay, so more severe Case A can be tolerated for the same user inconvenience requirements. Scheme II also has higher DG energy delivery, and further gains can be achieved since separation of trigger and continuous margins (Case C) allow strong overvoltage reduction without severe Case A. Finally, both schemes show reduced CO_2 emissions compared to unconstrained output. This is important, since high user subscription is required for scheme operation, and higher DG input promotes investment in renewable energy and helps deliver on emissions targets.

The third key tradeoff is between ICT investment and user inconvenience. Excessive Case B is undesirable since it may require extensive investment in ICT infrastructure and hardware. Excessive Case A is undesirable since it increases EV charging delay and reduces DG energy input. In Scheme I, these are the only latency-mitigation options, leading to the tradeoff. Scheme II gains strong advantage over this with Case C, and is able to achieve voltage control with low-severity A & B.

Scheme II can deliver better performance to the operator, users and investors without the need for a low-latency ICT system. Further, reduced user inconvenience encourages subscription, which is a key functional requirement. These offset costs to the operator from the added peak load. Ultimately, some compromise, where correction is applied up to a certain maximum load, may adequately marry the interdependent performance objectives of the operator and subscribing user.

ACKNOWLEDGMENTS

This work was supported by the European Commissions Horizon 2020 framework programme (H2020/2014-2020) under grant agreement no. 734325 TESTBED project (http://testbed-rise.com/), and by the UK EPSRC (grant no. EP/P005950/1).

REFERENCES

1. United Kingdom Government Digital Service.: Government Takes Historic Step Towards Net-Zero With End of Sale of New Petrol and Diesel Cars by 2030. Online, https://www.gov.uk/government/news/government-takes-historic-step-towards-net-zero-with-end-of-sale-of-new-petrol-and-diesel-cars-by-2030 (2020). Accessed 30 Nov 2020
2. Ofgem.: Typical Domestic Consumption Values. Online, http://www.ofgem.gov.uk/gas/retail-market/monitoring-data-and-statistics/typical-domestic-consumption-values (2018). Accessed 8 Sept 2018
3. Honda.: Honda Clarity Electric. Online, http://automobiles.honda.com/clarity-electric\#technology (2018). Accessed 3rd July 2018
4. Nissan.: Nissan LEAF. Online, https://www.nissan.co.uk/vehicles/new-vehicles/leaf.html (2018). Accessed 3rd July 2018
5. Chevrolet.: Chevrolet Bolt EV. Online, http://www.chevrolet.com/electric/bolt-ev-electric-car (2018). Accessed 3rd July 2018
6. Tesla.: Tesla Model S. Online, http://www.tesla.com/models (2018). Accessed 3rd July 2018
7. Deilami, S., et al.: Real-time coordination of plug-in electric vehicle charging in smart grids to minimise power losses and improve voltage profile. IEEE Trans. Smart Grid. 2(3), 456–467 (2011)
8. Masoum, A.S., et al.: Online coordination of plug-in electric vehicle charging in smart grid with distributed wind power generation systems. In: IEEE PES General Meeting Conference Exposition. (Online, 2014). pp. 1–5. National Harbor, MD (2014)
9. Veldman, E., Verzijlbergh, R.A.: Distribution grid impacts of smart electric vehicle charging from different perspectives. IEEE Trans. Smart Grid. 6(1), 333–342 (2015)
10. Department for Business.: Energy & Industrial Strategy. Digest of United Kingdom Energy Statistics (DUKES). Online. https://www.gov.uk/government/statistics/digest-of-uk-energy-statistics-dukes-2020 (2020). Accessed 1st October 2020
11. ExtraLink.: New Figures Reveal 6% Rise Year on Year in Largely 'invisible' Embedded Energy Generation. http://www.electralink.co.uk/2017/05/new-figures-reveal-6-rise-year-year-largely-invisible-embedded-energy-generation/ (2017). Accessed 29th February 2018
12. National Grid.: Future Energy Scenarios. Online. https://www.nationalgrideso.com/future-energy/future-energy-scenarios/fes-2020-documents (2020). Accessed 21st November 2020
13. Ebad, M., Grady, W.M.: An approach for assessing high-penetration PV impact on distribution feeders. Elec. Power Syst. Res. 133, 347–354 http://www.sciencedirect.com/science/article/pii/S0378779615004034 (2016). Accessed 14th March 2017
14. North American Electric Reliability Corporation (NERC).: Special Report: Accommodating High Levels of Variable Generation to Ensure the Reliability of the Bulk Power System, 104. http://www.nerc.com/files/IVGTF_Report_041609.pdf (2009). Accessed 6 July 2021
15. Katiraei, F., Agüero, J.: Solar PV integration challenges. IEEE Power Energy Mag. 9(3), 62–71 (2011)
16. Ismael, S.M., et al.: State-of-the-art of hosting capacity in modern power systems with distributed generation. Renew. Energy. 130, 1002–1020 (2019)
17. Crozier, C., et al.: Coordinated electric vehicle charging to reduce losses without network impedances. IET Smart Grid. 3, 677–685 (2020)
18. Tahir, A., Massoud, A.: Load shedding and forecasting in distribution systems with PV-based distributed generation and electric vehicles. In: 2017 4th International Conference on Information Technology, Computer, and Electrical Engineering (ICITACEE), pp. 71–76. Semarang, Indonesia, Online (2017)
19. Eajal, A.A., et al.: Fuzzy logic-based charging strategy for electric vehicles plugged into a smart grid. In: Proceedings of 2015 IEEE International Conference on Smart Energy Grid Engineering (SEGE), pp. 1–6. Oshawa, Canada, Online (2015)
20. Rassaei, F., Soh, W.-S., Chua, K.-C.: Demand response for residential electric vehicles with random usage patterns in smart grids. IEEE Trans. Sustain. Energy. 6(4), 1367–1376 (2015)
21. Akhtar, Z., et al.: Comparison of point-of-load vs. mid feeder compensation in LV distribution networks with high penetration of solar

photovoltaic genertation and electric vehicle charging stations. IET Smart Grid. 2(9), 283–292 (2019)
22. Stanev, R.: A control strategy and operation paradigm for electrical power systems with electric vehicles and distributed energy resources. In: 2016 19th International Symposium on Electrical Apparatus and Technologies (SIELA). pp. 1–4 Online (2016)
23. Meyer, D., Wang, J.: Integrating ultra-fast charging stations within the power grids of smart cities: a review. IET Smart Grid. 1(1), 3–10 (2018)
24. Bilal, M., Rizwan, M.: Electric vehicles in a smart grid: a comprehensive survey on optimal location of charging station. IET Smart Grid. 3(12), 267–279 (2020)
25. Alyousef, A., de Meer, H.: Design of a TCP-like smart charging controller for power quality in electrical distribution systems. In: Proceedings of the Tenth ACM International Conference on Future Energy Systems. E-Energy 19, pp. 128–138.ACM, New York (2019)
26. Ardakanian, O., Keshav, S., Rosenberg, C.: Real-time distributed control for smart electric vehicle chargers: from a static to a dynamic study. IEEE Trans. Smart Grid. 5(5), 2295–2305 (2014)
27. Robinson, A.P., et al.: Analysis of electric vehicle driver recharging demand profiles and subsequent impacts on the carbon content of electric vehicle trips. Energy Pol. 61, 337–348 (2013)
28. Zimmerman, J.P., et al.: Household Electricity Survey a Study of Domestic Electrical Product Usage (R66141 Final Report Issue 4), pp. 213–214. Intertek Testing & Certification Ltd, Milton Keynes, UK (2012)
29. Palmer, J., Cooper, I.: United Kingdom Housing Energy Fact File. vol. 46, pp. 49. Department of Energy & Climate Change, Cambridge, UK (2013)
30. Evans, A., et al.: National Travel Survey: England 2017. Department for Transport, Statistical Release: Table NTS9902 (2017)
31. Crossland, A.: MyGridGB. https://www.mygridgb.co.uk/about/ (2020). Accessed 5 Jan 2020
32. Heron, J.W., Sun, H.: Smart electric vehicle charging with ideal and practical communications in smart grids. In: 2019 IEEE Global Communications Conference (GLOBECOM), pp. 1–6. Waikoloa, HI, Online (2019)
33. Low, S.H.: Convex relaxation of optimal power flow-Part I: formulations and equivalence. IEEE Trans. Control Netw. Syst. 1(1), 15–27 (2014)
34. Baran, M.E., Wu, F.F.: Network reconfiguration in distribution systems for loss reduction and load balancing. IEEE Trans. Power Delivery. 4(2), 1401–1407 (1989)
35. Zimmerman, R.D., Murillo-Sánchez, C.E., Thomas, R.J.: MATPOWER: steady-state operations, planning, and analysis tools for power systems research and education. IEEE Trans. Power Syst. 26, 12–19 (2011)
36. Srikantha, P., Kundur, D.: Intelligent signal processing and coordination for the adaptive smart grid: an overview of data-driven grid management. IEEE Signal Process Mag. 36(3), 82–102 (2019)
37. Shayani, R.A., de Oliveira, M.A.G.: Photovoltaic generation penetration limits in radial distribution systems. IEEE Trans. Power Syst. 26(3), 1625–1631 (2011)
38. LDT TURBINE SCADA-1SEC. Online. https://pod.ore.catapult.org.uk/product/2 (2020). Accessed 10th November 2020
39. Vestas V164-8.0. Online. https://en.wind-turbine-models.com/turbines/318-vestas-v164-8.0 (2020). Accessed11th November 2020
40. Seguin, R., et al.: High-Penetration PV Integration Handbook for Distribution Engineers. National Renewable Energy Laboratory (2016)
41. Heron, J.W., et al.: Demand-response round-trip latency of IoT SmartGrid network topologies. IEEE Access. 6, 22930–22937 (2018)
42. Open ADR Alliance. Open Automated Demand Response. Online. https://www.openadr.org (2019). Accessed 23rd September 2019
43. Open Charge Alliance. Open Charge Point Protocol 2.0. Online. https://www.openchargealliance.org/protocols/ocpp-20/ (2018). Accessed 19th September 2019

How to cite this article: Heron JW, Sun H, Alizadeh-Mousavi O, Crossland A. Key performance-cost tradeoffs in smart electric vehicle charging with distributed generation. *IET Smart Grid*. 2021;1–21. https://doi.org/10.1049/stg2.12041